THE JOURNAL OF PHYSICAL CHEMISTRY B

Article

pubs.acs.org/JPCB

Exciton Description of Chlorosome to Baseplate Excitation Energy Transfer in Filamentous Anoxygenic Phototrophs and Green Sulfur Bacteria

Juha M. Linnanto[†,‡] and Jouko E. I. Korppi-Tommola*[,†]

[†]Department of Chemistry, P.O. Box 35, University of Jyväskylä, FIN-40014, Finland

[‡]University of Tartu, Institute of Physics, Riia 142, EE-51014 Tartu, Estonia

Supporting Information

ABSTRACT: A description of intra-chlorosome and from chlorosome to baseplate excitation energy transfer in green sulfur bacteria and in filamentous anoxygenic phototrophs is presented. Various shapes and sizes, single and multiwalled tubes, cylindrical spirals and lamellae of the antenna elements mimicking pigment organization in chlorosomes were generated by using molecular mechanics calculations, and the absorption, LD, and CD spectra of these were predicted by using exciton theory. Calculated absorption and LD spectra were similar for all modeled antenna structures; on the contrary, CD spectra turned out to be sensitive to the size and pigment orientations in the antenna. It was observed that, bringing two tubular antennae at close enough interaction distance, the exciton density of the lowest energy state became localized on pigments facing each other in the antenna dimer. Calculations predicted for stacked tubular antenna elements extremely fast, faster than 500 fs, intra-chlorosome energy transfer toward the baseplates in the direction perpendicular to the chlorosome long axis. Downhill excitation energy transfer according to our model is driven by interactions of the antennae with their immediate surroundings. Energy transfer from the chlorosome to the baseplate, consisting of 2D lattices of monomeric and dimeric bacteriochlorophyll *a* molecules, was predicted to occur in 5−15 ps, in agreement with experimental findings. Advancement of excitation through a double tube antenna stack, a model for antenna element organization in chlorosomes of green sulfur bacteria, to a monomeric baseplate was visualized in space and in time.

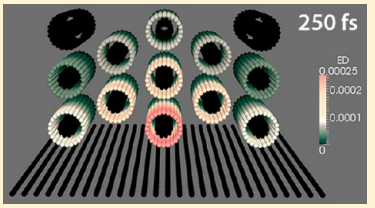

1. INTRODUCTION

The principal light harvesting apparatus in three phyla of bacteria consists of pigment filled vesicles called chlorosomes. The chlorosome is surrounded by an envelope, which contains an additional antenna complex, called the baseplate, located on the surface toward the cytoplasmic membrane and consisting of a two-dimensional paracrystalline array of pigments.[1] In green sulfur bacteria (GSB), an additional accessory antenna complex, Fenna−Matthews−Olson (FMO) bacteriochlorophyll *a* (Bchl *a*) protein, is located between the chlorosome and the cytoplasmic membrane. According to present understanding, the FMO protein in green sulfur bacteria links the baseplate complex to a membrane bound type-I reaction center (RC) complex (Figure 1). Similar pigment organization has been reported to exist in "*Candidatus Chloracidobacterium thermophilum*" in the phylum *Acidobacteria*.[2] In filamentous anoxygenic phototrophs (FAP) of phylum *Chloroflexi* (formerly known as green non-sulfur bacteria), the baseplate is connected to the B808−866 complex, an integral membrane antenna component that serves as an interface between the baseplate and the type-II RC complex (Figure 1).

Chlorosomes are heterogeneous ellipsoidal objects. Native chlorosomes vary in size from about 98 × 38 × 11 nm^3 to 209 × 104 × 29 nm^3 in length, width, and height, respectively. Chlorosomes are the largest and their pigment density is by far the highest of all known light harvesting antennae in Nature.

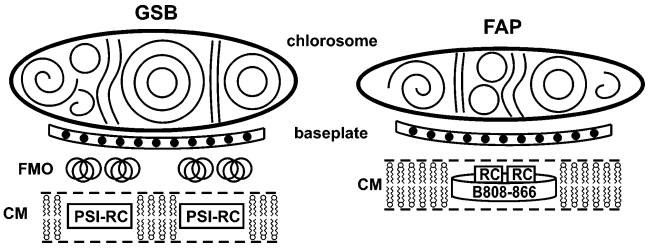

Figure 1. Schematic presentations of the photosynthetic units of GSB (left) and FAP (right) including the models for chlorosomal antenna elements used in the present work.

They contain tightly aggregated pigments, which are surrounded by a lipid−protein monolayer envelope with a thickness of about 3 nm.[3−14] Most common pigments of the chlorosome are Bchl's *c*, *d*, or *e*, carotenoids, as well as to a small extent Bchl *a*.[4,12] Excitonically coupled Bchl's, as evidenced by the large red shift of the Q_y transtion, form highly ordered self-aggregates in the chlorosome and funnel excitation energy to a much more sparsely pigmented baseplate

Special Issue: Rienk van Grondelle Festschrift

Received: January 31, 2013
Revised: July 10, 2013

   dx.doi.org/10.1021/jp4011394 | *J. Phys. Chem. B* XXXX, XXX, XXX−XXX

consisting of a lattice of Bchl *a* molecules.[15,16] It is the main purpose of this paper to present a comprehensive model for intra-chlorosome and from chlorosome to the baseplate excitation energy transfer (EET).

Atomic structures of pigment organizations in chlorosomes are not known. For a long time, it has been assumed that stacked tubular Bchl self-aggregates fill in the interior of the chlorosome vesicle. These early low resolution electron microscopy (EM) studies suggest diameters of 5−10 nm and lengths of 100−300 nm of the aggregates.[3,4,7,17,18] In chlorosomes of GSB, the aggregates have been reported to be roughly 2 times larger in diameter than in chlorosomes of FAP.[18] The aggregates of the chlorosomes of GSB are hollow with a hole diameter of about 3 nm.[3,10,17] Recently, multilayered cylindrical and/or lamellar organizations of Bchl's in the chlorosome have been resolved from cryo-electron microscopy images and about 2 nm spacing between the aggregates determined from X-ray scattering studies.[19−22] Relative abundancies of cylindrical or lamellar antenna elements in the chlorosome seem to depend on the preparation methods.[23] The distance between the aggregates (1.2−3.5 nm) has been shown to depend on the length of the hydrocarbon tail of the Bchl at position C-17.[24]

In wild type chlorosomes, the organization of Bchl's has been found to be somewhat heterogeneous. Efforts have been taken to generate mutants of *Chlorobaculum tepidum* that have a homogeneous Bchl organization. By combining the results from two bioimaging techniques, solid state NMR and cryoEM, a computer generated syn−anti stacking aggregation model for the antenna elements, where Bchl *c* or *d* assemble into coaxial cylinders to form tubular-shaped elements, has been proposed. Authors suggest that close packing of Bchl's via stacking and helical H-bonding networks form the basic structures of antenna elements responsible for EET in both the mutant and WT chlorosomes.[25] Organization of Bchl's in chlorosomes seems to be an inherent property of the porphyrin type pigments, since several chlorophyll derivatives have been found to form rod/tubular shaped self-aggregates in solution.[26]

Monomeric and dimeric Bchl *a* molecules are believed to be organized into periodic 2D planar structures in the baseplates of FAP and GSB, respectively. The baseplate proteins binding the Bchl *a*'s in the baseplates are structurally different.[27] According to linear dichroism (LD) spectroscopic data,[28,29] the Q_y transition dipole vectors of Bchl *a* molecules of the baseplates are almost in perpendicular orientation with respect to the plane of the baseplate. Recently, a model structure for the baseplate of the chlorosome of *Cba. tepidum* has been presented.[30] According to the model, Bchl *a* molecules are non-covalently bound to the histidine residue of the CsmA protein of the baseplate and CsmA−Bchl *a* units form dimers with two closely spaced Bchl *a* molecules sandwiched between two CsmA proteins. The CsmA protein dimers then form oligomers, which organize into a large 2D lattice with alpha helixes of the CsmA's oriented parallel to the baseplate surface and the monomeric Q_y transition dipole vector of the Bchl *a* molecules oriented almost perpendicular with respect to the baseplate surface.[30]

Femtosecond time-resolved measurements for chlorosomes of FAP containing Bchl *c* molecules show multiexponential Q_y excited state decay that can be fitted with time constants of 50−100 fs, 1−2 ps, 7−20 ps, and 90−150 ps at room temperature (RT). The decay remains multiexponential also at low temperatures.[31,32] For chlorosomes of GSB, Q_y excited state multiexponential decay time constants ranging from 200 to 300 fs to 30−40 ps at RT have been reported.[33,34] Under annihilation-free conditions, the time constants range from 200 to 500 fs to 120−130 ps for chlorosomes of *Cb. phaeobacteroides* at RT.[35] In chlorosomes of *Cb. limicola*, that contain a mixture of Bchl *d* and Bchl *c* molecules, a 4 ps time constant has been assigned to from Bchl *d* to Bchl *c* EET at low temperatures.[36] Similar time constants of 5−6 ps have been assigned to the lifetime of the lowest exciton state of chlorosomes of *Cba. tepidum* from hole burning experiments at 4.2 K.[34] Excitation energy transfer times of 200−300 fs and 9.2 ps of intra-chlorosome and from chlorosome to baseplate EET processes for FAP *Cf. aurantiacus*, respectively, have been reported.[37] Slightly faster transfer time constants have been found for chlorosomes of *Cba. tepidum* and *Pst. aestuarii*, 117−270 fs (intra-chlorosome) and 6−12 ps (chlorosome to baseplate), respectively.[38] Very recently, two-dimensional electronic spectroscopy studies reported sub-100 fs exciton diffusion times in chlorosomes of FAP *Cf. aurantiacus* and GSB *Cba. tepidum*.[39] Excited state lifetimes of Bchl *c* aggregates of chlorosomes seem to depend on growth conditions and become longer for chlorosomes grown under high light conditions.[40−42] EET rates from chlorosome to baseplate on the contrary for chlorosomes grown under bright light become faster than for chlorosomes grown under low light conditions.[43] EET rates of a chlorosome depend also on the type of pigments present in the antenna.[44] Intra-chlorosome EET becomes faster in the order of Bchl *e* > Bchl *d* > Bchl *c* in chlorosomes containing these pigments.[44] From the above discussion, it is clear that in most cases Q_y state excitation decay in any chlorosome is a multiexponential (or even not exponential at all) event and assignment of the resolved time constants to a particular EET process is a difficult task. An obvious reason for the temporal complexity of EET processes described is the heterogeneity of pigment organization in chlorosomes.

Since atomic details of chlorosomal antenna structures are not available (and probably never will), creation of computational virtual structures seems to be one of the most viable means to study EET processes in antenna elements and their assemblies in chlorosomes. In this work, a number of different computer generated models of the antenna elements have been created and their optical spectra calculated.[35,45−52] Due to the extremely large number of pigments in the real chlorosome or even in a single antenna element, quantum chemical approaches to simulate their spectroscopic properties and EET rates were out of the question. To be able to include representative enough numbers of pigments in the modeled aggregates (the maximum size of an aggregate modeled contained 12000 pigments), vibronic or phonon or charge transfer related interactions that can be included in modeling of smaller systems[53−55] had to be left out. We adopted the classical exciton Hamiltonian approach with provision to estimate local interactions by quantum chemical methods.[53,56−62] Vibronic interactions and system inhomogeneity are accounted for, though not included in the exciton Hamiltonian, in Monte Carlo type random variation of diagonal and off diagonal elements of the exciton matrixes. To calculate EET rate constants, the relevant excitonic states were dressed with Lorenzian line shapes having experimentally observed homogeneous line widths. The line shape function itself did not play a crucial role in evaluation of the rate constants.

The paper is organized as follows: (1) structural models of antenna elements and baseplates, (2) computational methods,

dx.doi.org/10.1021/jp4011394 | J. Phys. Chem. B XXXX, XXX, XXX−XXX

(3) exciton states of single antenna elements, (4) excition states of dimeric antenna elements, (5) modeling environmental effects, (6) calculation of intra-chlorosome and from chlorosome to baseplate EET rate constants, (7) visualization of spatial and temporal advancement of excitation from chlorosome to baseplate. The Supporting Information contains detailed numerical and 2D graphical results of the simulations.

2. PIGMENT ORGANIZATIONS AND INTERACTIONS

2.1. Antenna Structures. As models for Bchl organization in chlorosomes, stacked antenna elements, rods, spirals, or lamellae were considered. Linear Bchl arrays containing from 10 up to 275 Bchl *c*'s were used as building blocks for the antenna elements (Figure 2 and Table 1).

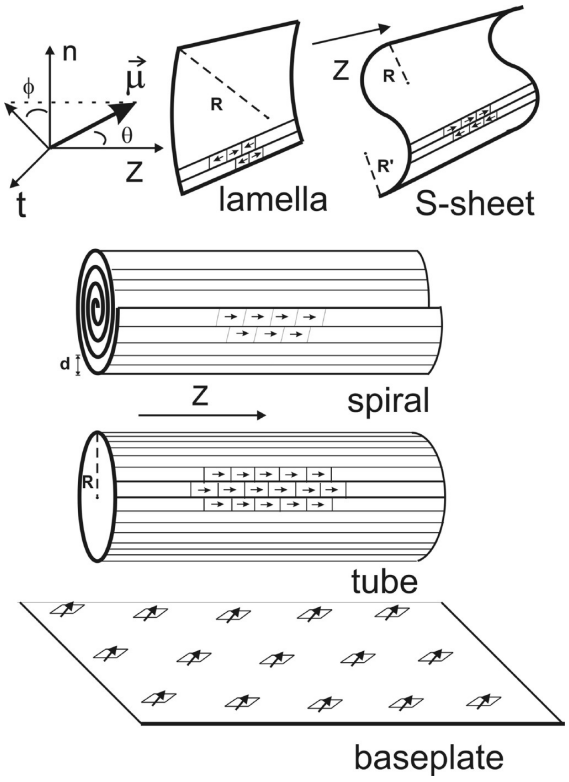

Figure 2. Schematic presentations of the antenna element structural models and a 2D baseplate structure used in the exciton calculations. Given are the parameters used to define the sizes and the shapes of the antenna elements. The coordinate system used to define the orientations of the transition moments is as follows: Z defines the orientation of the main axis of the antenna complex, n and t are the normal and the tangential vectors with respect to the antenna surface.

The inter-molecule Mg−Mg distance of the adjacent Bchl's in an array was set to 0.68 nm in a binding configuration (line A in Figure 3, energy was minimized at the molecular mechanics level of calculation),[52] where a Bchl is connected via a hydroxyl group at the 3^1-position to the central Mg atom of the adjacent Bchl.[50] Experimental evidence for such binding has been obtained from nuclear magnetic resonance studies.[46,63,64] Adjacent pigment arrays were shifted by 0.34 nm with respect to each other. Inter-Bchl Mg−Mg distances between the adjacent arrays varied in the range 0.88−0.97 nm (line B in Figure 3). The closest distance between chlorin planes in adjacent arrays was about 0.35 nm (line C in Figure 3). The shortest arrays modeled were about 6 nm in length, the longest 190 nm, a length of a real chlorosome.[18] Two Bchl *c* transition moment orientations, 20 and 5° with respect to the main axis, were considered (angle θ in Figure 2).

Antenna elements with different diameters or widths were generated by bringing in a proper number of Bchl arrays at interaction distances and the energy minimized at molecular mechanics level of calculation. For example, to obtain a rod antenna element with a diameter of 4.9 nm (Mg−Mg distance), a mimic for antenna elements in chlorosomes of FAP,[18] 16 linear Bchl *c* arrays were used to form a closed tubular surface. For multiwall rod antennae (up to four tubes), the inter-wall distance was set to 2.0 nm and the number of arrays was adjusted accordingly in each tubular layer. Two cylindrical spiral Archimedean spiral aggregates with 2.0 nm surface distance were studied, one an ideal Archimedean spiral and the other a "smooth" Archimedean spiral with four innermost pigment arrays removed. The phytyl tails of Bchl's were oriented toward the space between the spiral surfaces. The diameters of the spirals were varied from 5 to 13 nm. Slightly curved and planar pigment organizations were used as models for lamellar antenna elements (curvature radius of about 900 nm, *R*, in Figure 2). The widths of these lamellae were set to about 16 nm, roughly the height of a native chlorosome.

Stacks of the antenna elements were used as models for overall pigment organization in the chlorosome and exciton energies and excitation transfer rates in such assemblies calculated. It is noted that filling the approximate volume 40 × 60 × 160 nm^3 of chlorosomes of *Cfx. aurantiacus* with single wall rods of about 5 nm in diameter and about 160 nm in length resulted in a total number of pigments in the chlorosome of about 200 000, in agreement with an experimental determination.[65]

2.2. Baseplate Structures. Monomeric and dimeric Bchl *a* baseplate structure models were created. The dimensions of the baseplate lattices were set to 50 nm × 200 nm, roughly the estimated width and length of a real baseplate.[6,66] In the monomeric baseplate (mBP), Bchl *a* molecules formed a 2D planar cubic lattice with an inter-molecule distance of 2.0 nm. Only the unimolecular layer of pigments in the lattice was considered. Exciton energies with θ equal to 90, 80, 40, and 0° between the Bchl *a* Q_y transition dipole vector and the plane of the baseplate were evaluated keeping angle ϕ fixed at 0° (definitions of angles θ and ϕ are shown in Figure 2). Experimentally, a spread of θ angles from 55 to 99° has been reported in the literature.[28,29,33,67,68] In the dimeric baseplate (dBP), two mirror image Bchl *a* molecules formed the dimer unit with intra-dimer and inter-dimer distances of 1.8 and 3.1 nm in the 2D lattice, respectively.[30] The Q_y transition dipole vectors of the two mirror image Bchl *a* molecules were set to angles of θ_1 = 80° and θ_2 = 100° with respect to the plane of the baseplate. The monomeric Q_y transition energy of 792 nm, the transition dipole orientation of θ = 90°, and the absolute value of the transition dipole of 6.14 D for Bchl *a* put the absorption maximum of mBP to about 795 nm in agreement with the experimental results.[69] For dBP, the calculated absorption wavelength was almost unchanged (Figure 6AS to 6CS, bottom rows).

2.3. Antenna Interactions. Interactions between an antenna element and its nearest environment (chlorosome envelope or baseplate) were modeled by perturbing monomeric Q_y transition energies and the Q_y transition dipole moments in arrays of Bchl's of the antenna facing the environment. It is most likely that an antenna element next to the chlorosome

dx.doi.org/10.1021/jp4011394 | J. Phys. Chem. B XXXX, XXX, XXX−XXX

Table 1. Structural Parameters of the Rod, Spiral, and Sheet Aggregates of Bchl c

rod diameter (with respect to Mg atoms)	2.9, 4.6, 6.9, 10.3, and 14.3 nm
spiral diameter (with respect to Mg atoms)	2.8, 5.0, 7.0, 9.0, 11.0, and 13.0 nm
width of the 2D sheet structure (with respect to Mg atoms)	16.2 nm
length of the aggregate (with respect to Mg atoms)	6.5−186.3 nm (10−275 Bchl's)
number of the linear Bchl *c* arrays	rod: 10, 16, 24, 36, and 50
	spiral: 9, 18, 30, 46, 6-5, and 88
	2D lamellar structure: 19
distance between nearest chlorins (Mg−Mg distance) of array	0.68 nm
distance between nearest chlorins in adjacent arrays	0.88 nm
shift between adjacent arrays	0.34 nm
absolute value of the transition dipole vector $\|\vec{\mu}\|$	5.5 D
angle between $\vec{\mu}$ and symmetry axis (Z) of the rod/spiral (main axis of the sheet) (θ)	5 or 20°
angle between a projection of $\vec{\mu}$ in the horizontal plane of the rod/spiral/sheet and normal to the surface of the rod/spiral/sheet (ϕ)	85°
monomeric transition energy of Bchl *c*	14993 cm^{-1} (667 nm)

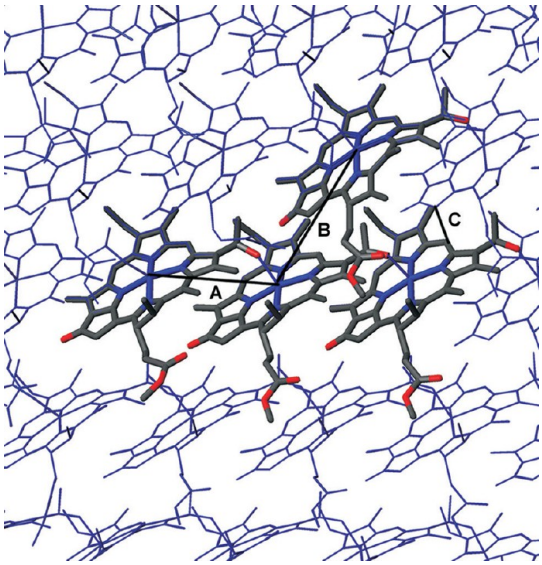

Figure 3. Local region of an antenna element surface. Line A measures the Mg−Mg distance between adjacent Bchl's in an array. Line B measures the closest Mg−Mg distance between Bchl's located in adjacent arrays, and line C gives the stacking distance, i.e., the closest distance between chlorin planes of adjacent arrays. Structures of antenna elements were optimized by using molecular mechanics calculations. (Hydrogen atoms and esterified alcohol tails of Bchl's are not shown.)

envelope or baseplate feels a different local electrostatic field than an element in the interior of the chlorosome. Such interactions modify energy levels, electron density distributions, and transition moments of the antenna.

At short enough distances, also the bulk antenna elements interact with each other. Antenna−antenna and antenna−baseplate interactions were calculated as a function inter-antenna distances (from 0.5 to 5.0 nm) by using dipole−dipole approximation. At short inter-antenna distances, exciton states of the interacting antenna become mixed and a superaggregate, an antenna dimer, is formed. Spectroscopic properties of such complexes would be markedly different from those of the isolated entities. Experimentally, it has been shown that absorption spectra of chlorosomes and *in vitro* Bchl self-aggregates are very similar.[70] Hence, interactions between antenna elements in the chlorosomes were considered as relatively weak and for this reason in the simulations only inter-rod distances longer or equal to 0.5 nm were considered. In all calculations, the antenna elements had ideal geometries; i.e., they did not contain any inhomogenieties, bubbles, holes, or edges. Inhomogeneities of the natural systems were accounted for in the simulations by randomly varying diagonal and off-diagonal elements of the exciton matrixes within predefined boundary conditions.

3. COMPUTATIONAL METHODS

3.1. Exciton Hamiltonian. Spectroscopic properties of the Bchl self-aggregates were evaluated by using exciton theory. The exciton Hamiltonian has the form[71]

$$\hat{H} = \sum_{m=1}^{N} \varepsilon_m \hat{B}_m^{\dagger} \hat{B}_m + \frac{1}{2} \sum_{\substack{m \neq 1 \\ m,l=1}}^{N} J_{ml} (\hat{B}_l^{\dagger} \hat{B}_m + \hat{B}_m^{\dagger} \hat{B}_l) \tag{1}$$

where $\varepsilon_m = \Delta\varepsilon_m + D_m + \delta_m$, $\Delta\varepsilon_m$ is the electronic excitation energy of a single molecule m, D_m is the so-called environmental shift,[72] δ_m is the shift induced by the surrounding matrix (e.g., solvent, protein, etc.),[56] J_{ml} is the matrix element of the interaction operator between molecules m and l, N is the number of molecules in the system, and the $\hat{B}_m$ operators are Pauli creation ($\hat{B}^{\dagger}$) and annihilation ($\hat{B}$) operators for excitons at molecule m. In the present case, the interaction is approximated with the dipole−dipole interaction. The dipole−dipole approximation is justified if the distance between pigments is larger than the physical size of these pigments. The matrix element has the form

$$J_{ml} \approx J_{ml}^{\mathrm{dip}} = \frac{1}{4\pi\varepsilon} \left[\frac{\vec{\mu}_m \cdot \vec{\mu}_l}{r_{ml}^{\,3}} - \frac{3(\vec{\mu}_m \cdot \vec{r}_{ml})(\vec{\mu}_l \cdot \vec{r}_{ml})}{r_{ml}^{\,5}} \right] \tag{2}$$

where $\vec{\mu}_l$ is the effective transition dipole moment vector in molecule l,[56,73] $\hat{r}_{ml}$ is the position vector between the two transition dipoles, r_{ml} is the distance between these dipoles, and ε is the dielectric constant. To take into account overlap between vibronic states present in electronic transitions, the transition dipole−transition dipole interaction strengths (J_{ml}) between Bchl *a* and *c* molecules were reduced 30% as compared to the transition dipole coupling strengths between identical pigment molecules. In this way, Franck−Condon factors of high vibrational levels are taken into account in the calculations of couplings between two different pigments.[74,75]

The eigenstates of this system are the ground state $|0\rangle_{\mathrm{agg}}$

dx.doi.org/10.1021/jp4011394 | J. Phys. Chem. B XXXX, XXX, XXX−XXX

$$|0\rangle_{agg} = |0_1, 0_2, ..., 0_N\rangle = \prod_{m=1}^{N} |0_m\rangle \tag{3}$$

and the exciton state $|\Psi_e\rangle$

$$|\Psi_e\rangle = \sum_{m=1}^{N} c_{em}|1_m\rangle_{agg} = \sum_{m=1}^{N} c_{em}\hat{B}_m^{\dagger}|0\rangle_{agg} \tag{4}$$

where c_{em} is the mth element of the eigenvector for the e exciton state. The inverse participation ratio (exciton length or area) of the eth exciton state is defined as

$$A_{ex}(e) = 1/[\sum_{m=1}^{N} (c_{em})^4] \tag{5}$$

Former studies have shown that the exciton description together with the dipole approximation have predicted chlorosome-like spectra correctly.[50,52] The molecular basis set picture lacks molecular overlaps and underestimates mixing of electronic states of the interacting pigments. Use of molecular basis set wave functions remains almost as the only available approach to allow study of aggregated molecular systems large enough to mimic *in vivo* systems like chlorosomes. Use of more complex exciton Hamiltonians, containing vibrational levels, system−bath interactions, etc., is also out of reach for the size of systems studied here, which means that the energy transfer rates calculated lack direct inclusion of vibration relaxation contributions and thermal disorder effects.

3.2. Calculation of Absorption, CD, and LD spectra. The Q_y band positions and intensities were calculated using the structural parameters of aggregates listed in Table 1. Excitonic energies were computed by diagonalizing the **H** matrix of eq 1. The diagonal energies were taken as the $S_0 \rightarrow S_1$ transition energies of monomeric pigments (see Table 1), and off-diagonal elements were calculated from eq 2 and by using the structural parameters of the aggregate. The values of transition dipole vectors were taken as 6.13 D for Bchl *a* and 5.5 D for Bchl *c* from experimental determinations.[76] The dielectric constant was set to $\varepsilon = 2.1$ $[\varepsilon_0]$ (typically used for proteins). To simulate the absorption, CD, and LD spectra, the following line shape functions were used:

Absorption line shape:

$$\sigma(\omega) = \sum_{e} \frac{2\mu_e^2}{\pi} \frac{\Gamma_e}{4(\omega - \omega_e)^2 + \Gamma_e^2} \tag{6}$$

CD line shape:

$$T(\omega) = \sum_{e} \frac{2R_e}{\pi} \frac{\Gamma_e}{4(\omega - \omega_e)^2 + \Gamma_e^2} \tag{7}$$

LD line shape:

$$\mathrm{LD}(\omega) = \sum_{e} \frac{2L_e}{\pi} \frac{\Gamma_e}{4(\omega - \omega_e)^2 + \Gamma_e^2} \tag{8}$$

where

$$\mu_e^2 = \sum_{k,l}^{N} |\vec{\mu}_k||\vec{\mu}_l|[\hat{\mu}_k \cdot \hat{\mu}_l] c_{ek} c_{el} \tag{9}$$

$$R_e = 1.7 \times 10^{-5} \nu_e \sum_{k,l}^{N} |\vec{\mu}_m||\vec{\mu}_l| R_{ml}[\hat{R}_{ml} \cdot [\vec{\mu}_m \times \vec{\mu}_l]] c_{em} c_{el} \tag{10}$$

$$L_e = \mu_{e,\|}^2 - \mu_{e,\perp}^2 \tag{11}$$

$$\mu_{e,\|}^2 = \sum_{m,l}^{N} |\vec{\mu}_m||\vec{\mu}_l|[\hat{\mu}_m \cdot \hat{\varepsilon}] c_{em} c_{el} \tag{12}$$

$$\mu_{e,\perp}^2 = \frac{1}{2} \sum_{m,l}^{N} |\vec{\mu}_m||\vec{\mu}_l|[\hat{\mu}_m \cdot \hat{\mu}_l - (\hat{\mu}_m \cdot \hat{\varepsilon})(\hat{\mu}_l \cdot \hat{\varepsilon})] c_{em} c_{el} \tag{13}$$

with ω_e being the eth exciton state energy, Γ_e its homogeneous width, $\vec{\mu}_l$ the effective transition dipole moment vector in molecule l,[56,73] $\hat{\mu}_l$ the unit vector in the direction of that transition, ν_l the energy (in cm^{-1}) of the transition on the lth molecule, $\hat{R}_{ml}$ the position vector between two dipoles, R_{ml} the distance between the dipoles, c_{el} the lth element of the eigenvector for the eth exciton state, and $\hat{\varepsilon}$ the unit vector in the direction of a macroscopically defined symmetry axis.[77]

To account for the inhomogeneous broadening of the spectral lines, a Gaussian random distribution of monomer transition energies and coupling constants of the exciton matrix were used to calculate the stick spectrum, which then was convoluted with a Lorentzian having a homogeneous line width of 100 cm^{-1} for all states in the spectral regions studied. For the diagonal matrix elements (monomer site energies), the fwhm of the Gaussian distribution was taken to be 200 cm^{-1}, and for off-diagonal elements, the width of disorder was taken to be 10% of the value of the interaction matrix element. Simulation of absorption, CD, and LD spectra of the single antenna elements included up to 5000 exciton matrixes, for which the eigenvalues and the eigenstates of the exciton Hamiltonian were solved. Simulations of largest pigment assemblies included up to 1000 exciton matrixes.

3.3. Calculation of the Excitation Energy Transfer Rate Constants. The excitation energy transfer rate constants were calculated by using the methods described by us previously.[53,57,59,61,79,80] Exciton basis functions, information on exciton energies, and calculated oscillation strengths of the transitions were used as input to the equation below[53,57,61]

$$W_{\{f\}\{i\}} = \sum_{\substack{f,i \\ f \neq i}} W_{fi} \approx \sum_{\substack{f,i \\ f \neq i}} \frac{2\pi}{h} |\sum_{\substack{m,l \\ m \neq 1}}^{N} c_{fm}^* c_{li} J_{ml}|^2 \delta(E_f - E_i) \tag{14}$$

The first step in the calculation of the EET rates was to estimate the overlap between the initial and final states $\delta(E_f - E_i)$ dressed with homogeneous line widths. A preset value of the overlap was used to select the states for EET calculation. The homogeneous width of each exciton state is considered as an indirect inclusion of phonon and vibration couplings in the system, though the Hamiltonian of eq 1 does not include such descriptions. By random variation of the exciton matrix elements, a distribution of rate constants from excitonic states chosen to be excited to the states chosen for the excitation to arrive was generated. Comparison with the experimental rates was obtained by fitting triple exponentials to these rate constant distributions (see Figure 4).

The homogeneous and inhomogeneous line widths used in the rate constant calculations were the same that were used to simulate absorption, CD, and LD spectra of the antenna elements. For Bchl *a*'s of the baseplate, the homogeneous width was set to 800 cm^{-1} to introduce non-zero overlap between antenna (initial) and baseplate (final) states and account for

dx.doi.org/10.1021/jp4011394 | J. Phys. Chem. B XXXX, XXX, XXX−XXX

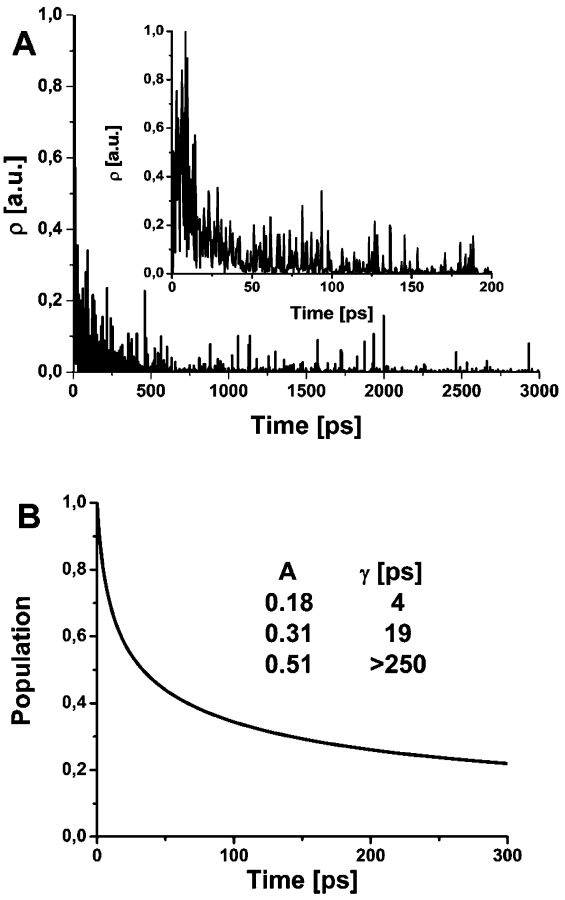

Figure 4. Typical distribution of calculated rate constants obtained from eq 14 (A) and a triple exponential fit to the corresponding population decay (B). "Noise" in the top figure is a result of random variation of the diagonal and off-diagonal elements of the exciton Hamiltonian. This particular simulation was made for EET from a single wall rod antenna with a diameter of 5 and 70 nm of length located on top of and parallel to a 2D dimeric Bchl *a* baseplate lattice with dimensions larger than the rod at a 2.5 nm inter-complex distance. The 250 ps component reflects EET from the rod to distant Bchl *a*'s of the baseplate. The amplitude of this component decreases as the size of the baseplate is made smaller.

probable vibronic interactions needed to make this EET step possible.

It is notable that our approach includes transitions also to the "dark" final or intermediate states, i.e., states which have zero or only very low oscillator strength in the ground state absorption.[57,61] Such states are not allowed in the classical Förster model often used to study EET processes in aggregated pigment systems.[81] Furthermore, the classical Förster model assumes that excitation is initially localized on a single chromophore, whereas the present model allows calculation of the EET rates for the system where the excitonic wave functions are delocalized over several pigments of the aggregate. As can be conduced from eq 14, delocalization lengths or areas of initial ($\{i\}$) and final ($\{f\}$) states are important contributors to EET rate constants (c_{fm} and c_{li} elements of the eigenvectors of exciton states in eq 14). They also determine efficiencies of excited state absorption (ESA) processes that may occur from excited exciton states.

3.4. Calculation of the Time Evolution of Exciton Density. The Markovian type energy transfer model between antenna complexes may be described as[59]

$$I \rightarrow [J] \rightarrow [L] \rightarrow [M] \rightarrow \cdots \tag{15}$$

where an exciton state of an antenna I is initially excited and only downhill energy transfer/relaxation processes are allowed to/via exciton states of complexes $\{J\}$, $\{L\}$, $\{M\}$, ... Then, population (exciton density) kinetics has the form

$$\frac{d[I]_t}{dt} = -\sum_n k_{J_nI}[I]_t \tag{16}$$

$$\frac{d[J_n]_t}{dt} = k_{J_nI}[I]_t - \sum_m k_{L_mJ_n}[J_n]_t \tag{17}$$

$$\frac{d[L_m]_t}{dt} = \sum_n k_{L_mJ_n}[J_n]_t - \sum_n k_{M_nL_m}[L_m]_t \tag{18}$$

$$\frac{d[M_n]_t}{dt} = \sum_m k_{M_nL_m}[L_m]_t - \sum_m k_{N_mM_n}[M_n]_t \tag{19}$$

where $[J_n]_t$ is the population (exciton density) of J_n complex at time t and $k_{L_mJ_n}$ is the calculated EET rate constant from J_n to L_m complex (eq 14). The rate constants from EET calculations were used to estimate spatial advancement of populations as a function of time in the studied pigment assemblies.

4. RESULTS

4.1. Exciton Energies of Antenna Elements. In Figure 5 are shown the low energy regions of the Q_y exciton energy levels of rod antenna elements (Figure 5, left), spiral aggregates (Figure 5, middle), and slightly curved lamellae (Figure 5, right) with total lengths of about 7, 13, 34, 71, 102, 136, and 187 nm. Computational parameters are given in the caption of Figure 5.

A red-shift of the Q_y transition of 1300 cm^{-1} (to 740 nm) for the shortest and 1900 cm^{-1} (to 750 nm) for the longest antenna with respect to the monomer absorption of Bchl *c* at 667 nm was predicted, irrespective of the geometrical shape of the antenna. The calculated band positions compare nicely to experimental absorption wavelengths from 740 to 750 nm reported for chlorosomes of FAP and GSB, respectively.[37,38] For antenna elements longer than 70 nm, the energy difference between the exciton state having the highest oscillator strength and the state with lowest energy became nearly zero. The energy level differences between these states for rod, sheet, and spiral aggregates were 170 to 0 cm^{-1}, 145 to 2 cm^{-1}, and 370 to 25 cm^{-1} for antenna 7 and 187 nm in length, respectively. In short antenna elements, the number and the energy spread of states below the absorbing state was much higher than that in the long antenna (Figure 5). The reason for such a behavior is probably related to the role of "end" pigments; in short antenna elements, contribution from these pigments is stronger than in long antenna. The energy difference between the absorbing state and the lowest exciton state in principle is a direct measure of the experimental Stokes shift. For the chlorosomes of *Cfx. auranticus*, the experimental Stokes shift is 267 cm^{-1}, which is comparable to the calculated energy difference of 228 cm^{-1} obtained for the spiral aggregate 12 nm in length (Figure 5b and Table 1CS in the Supporting Information). For rod antenna of similar length, a difference of 90 cm^{-1} was predicted.

dx.doi.org/10.1021/jp4011394 | J. Phys. Chem. B XXXX, XXX, XXX–XXX

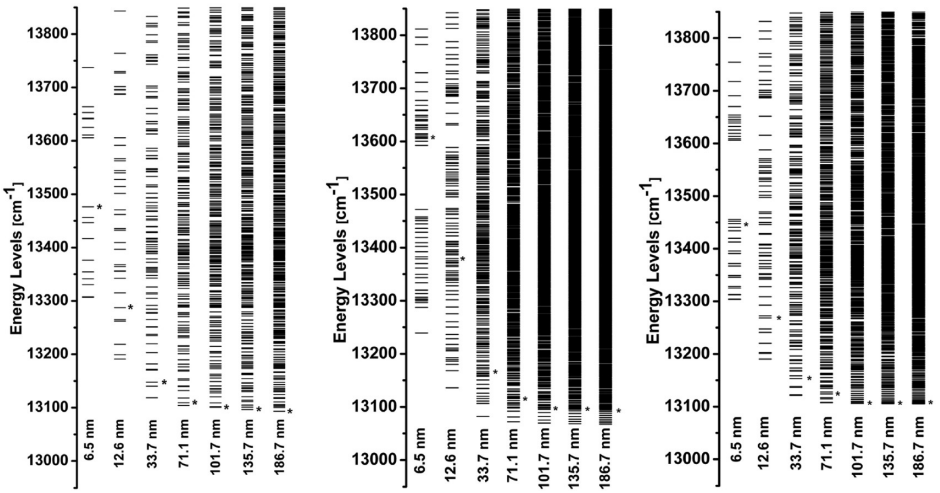

Figure 5. Calculated exciton energy levels (below 13850 cm^{-1}) of single wall rod antenna elements (left), cylindrical Archimedean spirals (middle), and lamellar antenna elements (right) of lengths of 7 nm (10 Bchl's in a single array), 13 nm (20 Bchl's), 34 nm (50 Bchl's), 71 nm (105 Bchl's), 102 nm (150 Bchl's), 136 nm (200 Bchl's), and 187 nm (275 Bchl's). Orientations of the individual pigments were defined by angles, $\theta = 20°$, $\phi = 85°$. Distances between the nearest chlorins in a pigment array and between the adjacent arrays were 0.68 and 0.88 nm, respectively. The spiral diameter was set to about 6 nm (2 turns, with 2.0 nm inter-sheet distances). The lamella width was set to 16.2 nm. The exciton states having a major contribution to the Q_y transitions are marked with an asterisk (*). Observe that the major absorbing state becomes the lowest exciton state for rod and lamella antenna elements longer than 100 nm.

In the perturbed antenna (Tables 1S, 2S, and 3S in the Supporting Information), similar shifts are seen for several antenna shorter than 20 nm. These results would suggest the presence of relatively short antenna elements in chlorosomes. However, inhomogeneity of the in vivo antenna elements, that were not studied here, could result in a distribution of the dark states below the absorbing state also in long antenna elements and results in larger Stokes shifts.

Increasing the diameter of tubular antenna of about 70 nm in length from 3 to about 15 nm increased the energy gap between the lowest exciton states and the absorbing states about 150 cm^{-1}, yet the energy of the lowest exciton state remained roughly constant (Figures 1AS and 1BS in the Supporting Information). The underlying reason for this shift is obviously connected to reduction of curvature of the aggregate surface, which changes the relative orientations of the transition moments of the pigments and hence the energetics of the aggregate. Calculations showed that the absorption and LD spectra of short and long lamellar and tubular aggregates with identical pigment orientations and lengths are nearly identical (Figures 4AS–4CS, Supporting Information). On the contrary, both the geometry and the size of the aggregate affect strongly the shape of the CD spectrum. CD intensities calculated for the planar or slightly curved lamellae are at least an order of magnitude weaker than the intensities calculated for tubular structures. Experimental CD intensities reported for chlorosomes are relatively strong, suggesting tubular rather than lamellar antenna organizations prevail in the chlorosomes.[37,38]

4.2. Exciton Densities in Antenna Elements. Exciton densities of the antenna elements were visualized both as 2D and 3D presentations for states having the lowest energy and the highest oscillator strength. 2D color presentations for the exciton densities of all antenna elements studied are shown in Figures 2AS–2FS in the Supporting Information. In rod antenna elements, the exciton density of the lowest exciton state showed helical patterns around the circumference of the rod (Figures 6 (bottom, left) and 2AS in the Supporting Information). Depending on the orientation of the transition

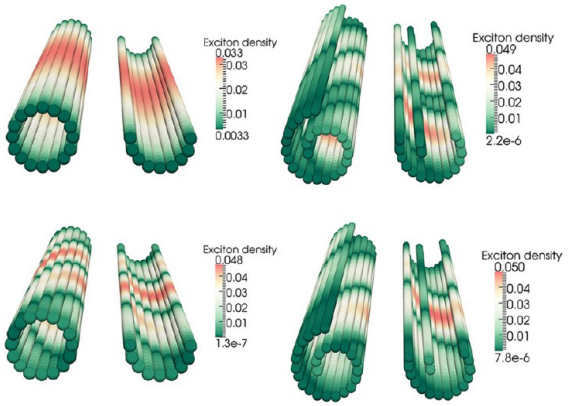

Figure 6. Exciton densities of the state with highest oscillator strength, the absorbing state (top images), and the lowest energy state (bottom images) of a rod antenna (left) and a smooth Archimedean spiral (right) both 70 nm in length. Right-hand images have been cut in half for clarity.

moment of the pigments (angle θ), a left- or right-handed helix will be observed. On the contrary, the exciton density of the state with highest oscillation strength was fully delocalized over the circumference of the rod (Figures 6 (top, left) and 2AS in the Supporting Information). In Archimedean spiral antennae, the density of the lowest exciton state was delocalized on the innermost Bchl *a* arrays of the spiral independent of the length of the antenna, while the density of the absorbing state was delocalized over the entire antenna surface in patchlike formations (Figure 2BS in the Supporting Information). In "smooth" spirals, the exciton densities of the lowest and absorbing states both show helical patterns up to a length of 150 nm (Figures 6 (right) and 2CS in the Supporting Information). For longer antenna, the main absorbing state is the lowest exciton state and exciton density is delocalized over the surface of the spiral (Figure 2CS (top image) in the Supporting Information). Increasing the diameter of 70 nm long "smooth" spirals resulted in patchlike formations of the

dx.doi.org/10.1021/jp4011394 | J. Phys. Chem. B XXXX, XXX, XXX–XXX

exciton density of the absorbing state (Figure 2FS in the Supporting Information, images 5π and 6π on top right). Planar or slightly curved lamellae showed periodic exciton densities for both the lowest energy and the absorbing states. It is noted that exciton density vanishes on the edges of a lamellar antenna (Figures 7 and 2DS in the Supporting Information).

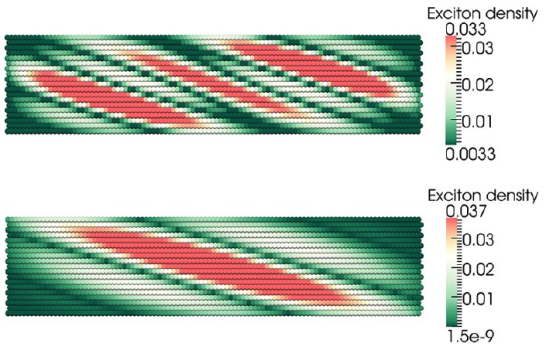

Figure 7. Exciton densities on a lamellae antenna element 70 nm in length. On the top is shown the exciton density of the state having the largest oscillator strength, the absorbing state, and on the bottom, the exciton density of the state having the lowest energy.

In ideal multiwall rod antenna elements, structures that have been seen in cryo-EM images of chlorosomes, the lowest exciton state is mainly localized on a tube next to the outermost tube (Figure 2ES in the Supporting Information). The main absorbing state is delocalized on the innermost tube and with exciton energy above the lowest state. *This means that, if the inner tube is excited, excitation will be transferred downhill toward the outer tubes.*

4.3. Perturbations in Antenna Elements. Ideal organization of antenna elements in the chlorosomes may be modeled as stacks of long tubular (rods and spirals) or lamellar (planar or slightly curved) Bchl aggregates (Figure 8). Tubular antenna next to the vesicular envelope or baseplate experience a different environment (regions *A* and *C* in Figure 8) than antenna inside the chlorosome (region *B* in Figure 8). Pigments in both ends of the antenna may also experience interaction different from the majority of the pigments of the antenna. In a parallel lamella organization, the first and last lamella in the stack experience a different environment than the lamellae in between. If the edges of the lamellae are in contact with the vesicle envelope, as proposed for example in ref 19, then pigments of the lamellae near the chlorosomal envelope and near the baseplate experience their own local environmental interactions (regions *A* and *C* in Figure 8). To describe these interactions, perturbations on the pigments of the antenna elements of lengths 12 nm (short) and 101 nm (long) were made. Perturbations were implemented by varying the diagonal elements of the exciton matrix, absolute values of transition moments, and orientations of the transition moments (angles θ and ϕ) most often in a single array of pigments of the aggregate, leaving the rest of the pigments unperturbed. Effects of perturbations were also studied on the end pigments of the rod antennae, but these turned out to have only very minor effects on the exciton states (Tables 1AS and 1BS in the Supporting Information). The numerical results from perturbation simulations are given in Tables 1S−4S of the Supporting Information.

In general, applied perturbations caused smaller effects in the long antenna than the short antenna. All perturbations applied

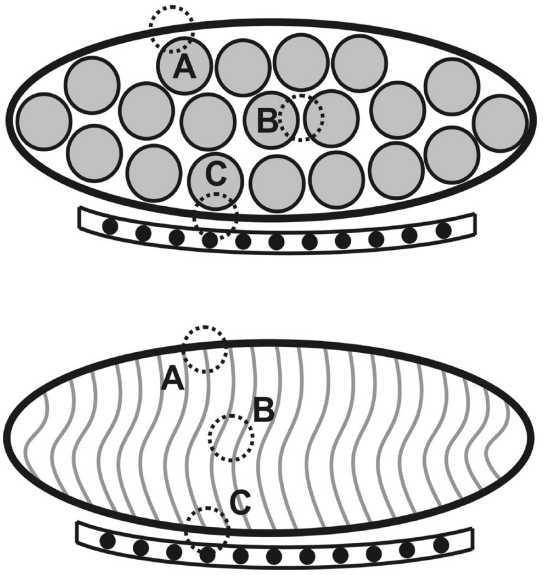

Figure 8. Schematic description of environmental interactions of the *A*, *B*, and *C* antenna elements. An *A* antenna element experiences interaction from the chlorosome envelope and from neighboring *A* and *B* elements, a *B* antenna (bulk antenna element) has from 6 to 7 *B* almost identical neighbors, and a *C* element interacts with neighboring *C* and *B* elements and the baseplate pigments.

left the energies of the main absorbing states in all of the studied antenna elements almost in tact (Tables 1AS−4FS in the Supporting Information). Red-shifting of the diagonal elements in a single array of an antenna from $\lambda^* = 667$ nm (solution wavelength for Bchl *c*) stepwise to 680 nm resulted, in all antenna studied, in (1) lowering of the energy of the lowest exciton state and (2) strong localization (reduction of exciton area) of the exciton density on the perturbed pigments (Figures 3AS−3CS and Tables 1AS−1FS in the Supporting Information). For rod and lamellar antenna, lowering and localization were clearly dependent on the value of the diagonal elements, with the effects becoming stronger when energies were shifted toward the red. Very similar effects were seen when the absolute value of the Q_y transition moments was increased from $\mu^* = 6.14$ D by 15−20% with the diagonal elements and transition moment orientations kept constant (Tables 2AS−2FS, Supporting Information). Change of the orientation of the transition moment from the reference value of $\theta^* = 20°$ to $\theta = 0°$ with diagonal elements at 667 nm and absolute dipole moment at 6.14 D also resulted in a red-shift and strong localization of the lowest exciton state as compared to the reference state (Tables 3AS−3FS, Supporting Information). Finally, changing the ϕ orientation from 70 to 100° resulted in very minor changes in the energies of the lowest energy and the absorbing exciton states or in localization of exciton density. (Tables 4AS−4FF, Supporting Informaiton). Described perturbations in principle could be induced in Nature by the local environment of the antenna in the chlorosome. The implied three perturbations (diagonal elements, μ, and θ) reduced the energy and localized the excition density of the lowest exciton state. Such perturbation in principle may serve as a mechanism for excitation energy transfer from a non-perturbed antenna to the perturbed antenna and vice versa.

Perturbations had only a small influence on the band shapes of the absorption and LD spectra of the rod, lamellar, or spiral

dx.doi.org/10.1021/jp4011394 | J. Phys. Chem. B XXXX, XXX, XXX−XXX

antenna elements (see Figures 4AS−4CS in the Supporting Information). The CD spectra did not change their shape for the perturbed rod and spiral antennae. However, the CD spectra of lamellae changed their band shape and gained in intensity due to perturbations (Figure 4CS, middle spectra in the Supporting Information). However, the absolute intensity of the perturbed lamella still remained way below the intensities of the CD spectra of tubular antenna.

4.4. Antenna−Antenna Interactions. In chlorosomes, cylindrical antenna elements or lamellae or a combination of cylindrical and lamella antenna are believed to form collinear antenna layers with about 2 nm distance between the antennae. As the first steps toward simulation of EET in a full size chlorosome, exciton interactions between two identical parallel antenna elements (rod, spiral, or sheet) and between two different antennae as a function of inter-antenna distances from 0.5 to 5.0 nm were studied. The calculations were done for short and long antenna dimers and at two orientations of the Q_y transition dipole vector, $\theta = 20$ and 5°. The numerical results of these simulations are given in Tables 5AS−5IS in the Supporting Information. Densities of the lowest exciton states of the modeled interacting antenna are given as 2D graphical presentations in Figures 5AS−5FS in the Supporting Information.

The major finding was that, as two identical tubular antennae (rods or spirals) were brought from infinity to 2.0 nm and further to 0.5 nm inter-antenna distance, *the exciton density of the lowest energy state accumulates on the pigments facing each other in the antenna dimer and the energy of the state was lowered as compared to isolated antennae* (Tables 5AS−5DS, Supporting Information). Densities of other exciton states were delocalized over the entire dimer with slightly higher density in the regions facing the neighboring rod. Such accumulation of exciton density provides a channel for excitation energy transfer from antenna to antenna as the coefficients of the exicton wave functions of the dimer contribute to excitation energy transfer rate constants (eq 14). At very short distances, the excitonic states of the rod dimer became strongly mixed and the relative exciton area of the lowest exciton state was reduced to 10% from that at 2.0 nm inter-rod distance. For two interacting spirals, opposite behavior was observed. The exciton area of the dimer increased as the inter-antenna distance was shortened (Figures 5AS−5CS and Tables 5CS−5DS in the Supporting Information). Dimer interaction was relatively stronger between short antennae than in long antennae. Interaction between two rod antenna depends on the orientation of the transition moment vectors and was much stronger in the dimer having $\theta = 5°$ than in the dimer for which $\theta = 20°$ (Tables 5AS−5BS, Supporting Information). Quite surprisingly, the antenna−dimer interaction has hardly any effect on the shape and position of the absorption, CD, and LD spectra (dimer spectra are shown in Figures 6AS−6BS and monomer spectra in Figures 4AS−4BS in the Supporting Information).

If two parallel lamellae are brought from infinity to a distance from 3.0 to 1.5 nm, the energy of the lowest exciton state is reduced (Tables 5ES and 5FS, Supporting Information) and the exciton density becomes smoothly spread and fully delocalized over both lamellae (Figures 10 (bottom) and 5DS in the Supporting Information). This is very different from rod−rod or spiral−spiral interactions that strongly localize the exciton density of the lowest exciton state on pigments facing each other in the dimer.

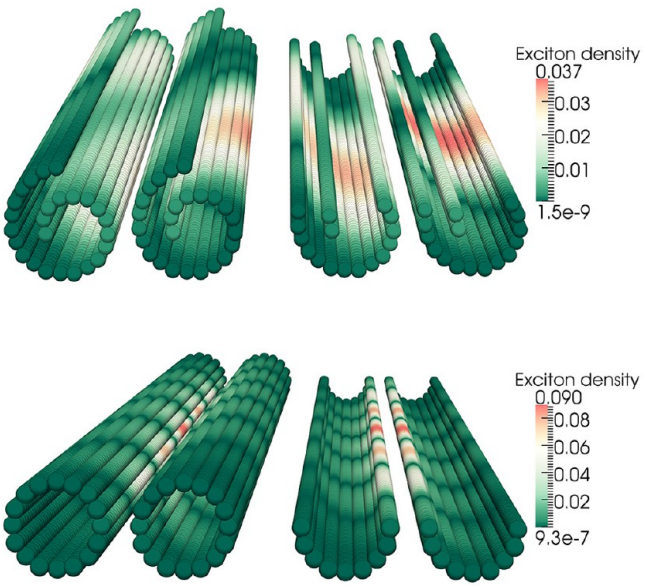

Figure 9. Exciton densities of the lowest exciton state of two interacting antenna elements: a single wall rod dimer (bottom); a dimer consisting of two smooth Archimedean spiral antenna elements (top). Inter-antenna separations were set to 0.5 nm and antenna lengths to about 70 nm. The diameters of the rod and spiral antennae were 5 and 6 nm, respectively. Sixteen Bchl *c* arrays of 105 Bchl's long were used to create the single wall rods; for spirals, 25 Bchl *c* arrays were needed. The images on the right-hand side have been cut in half to increase clarity.

Absorption and LD spectra of the lamellae dimers are very similar to the spectra of rod and spiral dimers. Differences were seen in the CD spectra. Spectra of the lamella dimers are shown in Figure 6CS and the corresponding monomer spectra in Figure 4CS.

Multiwall rods may be considered as a special case of interacting lamellae, since pigment distances between the adjacent walls are constant as in the lamella dimer. In multiwall rod dimers, the lowest exciton state is localized in the walls of the multiwall rods facing each other in a similar fashion as in single wall rod dimers. Since exciton localizations of the lowest exciton state of the multiwall rod dimer and lamellae dimer are very different, then EET in the two systems is expected to be clearly different. However, EETs between the concentric tubes of a multiwalled monomer and between two lamellae are expected to be similar.

Since high-resolution electron microscopy images suggest both tubular and lamellar type aggregates to be present in chlorosomes,[21,22] also rod−lamella and spiral−lamella interactions were modeled. At an inter-antenna distance of 2.0 nm, exciton densities of the lowest exciton states of tubular antennae oriented parallel to and on top of a lamella were delocalized, with slightly higher exciton density on pigments closest to the lamella (Figure 10, top). At shorter 0.5 nm inter-complex distances, localization became much stronger and the lowest exciton state was shifted from 100 to 250 cm^{-1} from the reference value when the antennae are at infinite distance from each other (Tables 5GS−5JS and Figures 5ES and 5FS in the Supporting Information).

The results of spectral simulations for rod−rod, lamella−lamella, and rod (spiral)−lamella complexes are shown in Figures 6AS−6BS in the Supporting Information. Calculated absorption, CD, and LD spectra, band positions, and band

dx.doi.org/10.1021/jp4011394 | J. Phys. Chem. B XXXX, XXX, XXX−XXX

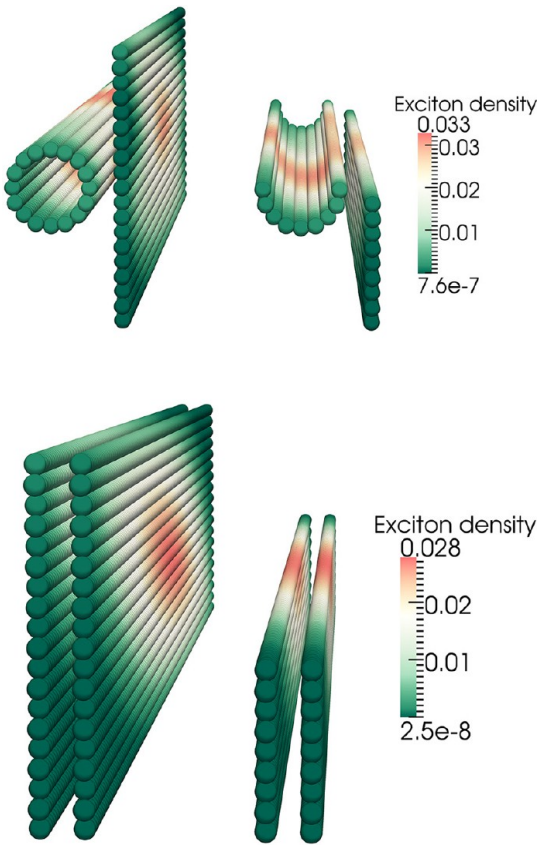

Figure 10. Exciton densities of the lowest exciton state of two identical and parallel lamellae (bottom) and a single wall rod antenna and a lamella (top). Lamella−lamella and rod−lamella distances were 1.5 and 1.0 nm, respectively. Lamellae in the lamella dimer had dimensions of 102 nm × 16 nm and were built from 19 Bchl *c* arrays of 150 Bchl's long. The rod−lamella dimer antenna element consisted of a rod antenna built from 16 and the lamella from 19 Bchl *c* arrays both 105 Bchl's long. The images on the right have been cut in half to increase clarity.

shapes of the complexes are much the same as what was obtained for isolated complexes. Because planar lamella geometry gives low rotation strength, the CD bands of rod (spiral)−lamella complexes are weaker than those of rod−rod or spiral−spiral complexes with similar pigment densities.

4.5. Antenna−Baseplate Interactions. Antenna−baseplate interaction was studied by constructing an excitonic system that consisted of a Bchl *c* rod, spiral, or lamella and a two-dimensional cubic baseplate lattice, containing either monomeric and dimeric Bchl *a*'s. Antennae were placed on top of the lattice and oriented parallel to the plane of the baseplate with dimensions of about 200 nm × 50 nm. The numerical results of these simulations and the simulation parameters are given in Tables 6AS−6FS in the Supporting Information. Calculated antenna−baseplate absorption, LD, and CD spectra are shown in Figures 6AS−6CS in the Supporting Information. In all cases, antenna−baseplate interactions turned out to be weak, with only minor effects on antenna transition energies, and did not depend on antenna length or orientation of the Bchl *a* transition moment. Densities of the lowest exciton states of the "hanging" antenna were almost identical to those of isolated antenna. At short antenna−baseplate distance (below 1.0 nm), the exciton density of rod antenna becomes clearly localized on pigments facing the baseplate (Table 6BS in the Supporting Information). Localization is stronger for long rod antenna than for short antenna (Tables 6AS−6BS in the Supporting Information). Characteristic Bchl *c* and Bchl *a* bands of the antenna and the baseplate, respectively, became nicely visible in the simulated absorption spectra (Figures 6AS−6CS, bottom images, in the Supporting Information). The simulated absorption, LD, and CD spectra much resembled the spectrum of chlorosomes of FAP[37] but did not give hints of the strong overlap of the Bchl *c* and Bchl *a* bands observed for chlorosomes of green bacteria.[38] This is expected, as the simulations only contained a single tubular antenna element and a baseplate and chlorosomes of GSB are believed to be filled with double or multiwalled tubules and to a smaller extent lamellae as well. CD spectra of lamella−dBP complexes showed changes in band shape and enhancement of intensity as compared to the CD spectra of lamella−dimer or lamella−mBP complexes (Figure 6CS, middle row, in the Supporting Information).

4.6. Interactions in Antenna Assemblies. Dimensions of chlorosomes vary from species to species. The average height of chlorosomes of GSB is larger than that of the chlorosomes of FAP as well as the average diameters of individual antenna elements. For a description of pigment organization in both chlorosomes, tubular antenna stacks of about 15 and 30 nm in height were created. In the former case, three antenna layers with an antenna diameter of 5 nm (mimicking antenna organization in chlorosomes of FAP) and in the latter case three antenna layers with an antenna diameter of 10 nm (mimicking antenna organization in chlorosomes of GSB) were assembled to form an excitonic light harvesting entity.

Three environments of tubular antenna elements of the created chlorosome antenna model were considered. These are labeled as *A*, *B*, and *C*, as illustrated in the schematic presentation of Figure 8. In the simulations, *A* and *C* type elements were spatially surrounded by four neighboring *B* antenna elements, *A*'s located next to the vesicular envelope and *C*'s next to the baseplate. In the simulations, type *B* elements were surrounded by six similar antenna elements from all sides. Calculations were done for short and long tubular antenna stacks. The inter-antenna distances were varied from 0.7 to 5 nm. Besides distance variation, also the effects of varying diagonal elements of the exciton matrix were studied for *A* type tubular antenna (Tables 7AS−7DS in the Supporting Information) and *C* type antenna (Tables 9AS−9DS in the Supporting Information). For the *B* type antenna, only the inter-antenna distance was varied and the results for the "bulk" antenna are shown in Tables 8AS−8DS in the Supporting Information. As reference parameters for a non-interacting system, $\lambda^* = 667$ nm and $\theta = 20°$ were used. Exciton density maps for the simulated multiantenna systems are shown in Figures 7AS−7CS in the Supporting Information.

In the simulation of a tubular (rod and spiral) *A* antenna interacting with its surroundings, the diagonal elements in a single pigment array of the antenna facing the chlorosome envelope were varied as descriptive of envelope interaction and the distance between the perturbed *A* antenna and its four neighboring *B* antennae was varied symmetrically (Tables 7AS−7DS in the Supporting Information). For a short *A* rod interacting with four short *B* rods, the main absorbing state was blue-shifted from the reference position of about 40 cm^{-1} at 2.0 nm and about 130 cm^{-1} at 1.0 nm distance with concomitant lowering of the energy of the lowest exciton state by 30 and 150 cm^{-1} (Table 7AS in the Supporting Information). The

dx.doi.org/10.1021/jp4011394 | J. Phys. Chem. B XXXX, XXX, XXX−XXX

wavelength of the state with highest oscillator strength was not much dependent on the perturbation imposed but much more dependent on the *A*−4*B* distance. For long *A* rod and both long and short *A* spirals, the corresponding shifts were much smaller with a general trend of increasing shifts as the values of the diagonal elements of the perturbed array of the antenna were shifted toward lower energy and the *A*−4*B* distance shortened. The results in Tables 7AS−7DS in the Supporting Information indicate that, even with no perturbation on *A* antenna, excitation of *A* antenna would lead to downhill energy transfer from *A* antenna to the surrounding *B* antenna at *A*−4*B* distances shorter than 2.0 nm. The driving force would be higher for short than for long rods and higher for rod antenna than for spiral antenna.

The exciton density of the state with highest oscillator strength of the *A*−4*B* assemblies was delocalized, mostly on the *A* antenna regions facing *B* neighbors but some density was also found in the regions facing the chlorosome envelope (Figures 7AS−7CS, top right corners). The density of the lowest exciton state of the *A* rod on the other hand was entirely localized in the pigment regions facing the *B* neighbors. For spirals, the corresponding distributions extend more toward the envelope side (Figures 7AS to 7CS, top left corners). If the diagonal elements of the *A* rod antenna on Bchl *c*'s facing the envelope are red-shifted from the reference value of 667 to 672 nm at 2.0 nm interaction distance or shorter, the lowest energy exciton state becomes localized in the region facing the envelope. Such perturbation would not direct excitation toward the baseplate.

Interaction of a *B* type tubular antenna, with its six *B* neighbors, was simulated in an effort to mimick bulk antenna. The distance between the center *B* antenna and its six neighbors was varied symmetrically from 1.0 to 5.0 nm. The orientation of the transition moment was set to $\theta = 5°$ for the short and long rods. In addition, results with $\theta = 20°$ were evaluated for short rods and the short and long spirals. The numerical results of these simulations are presented in Tables 8AS−8DS in the Supporting Information. Exciton density maps of the lowest exciton state and the state with largest oscillator strength are shown in middle images of Figures 7AS−7CS in the Supporting Information. The wavelength of the main absorbing band in all cases was blue-shifted as the interaction distance *B*−6*B* became smaller, with the shift being largest for the short 12 nm rod assembly. The energy of the lowest exciton state of the assembly is lowered as the interaction distance becomes shorter, more strongly for short than for long antenna and more strongly for the rod than for the spiral antenna. The exciton density of the main Q_y absorbing state of the *B* rod antenna was delocalized and accumulated in the regions facing the surrounding *B* rods and was also dependent on whether the neighbor *B* was on the *A* (envelope) or *C* (baseplate) side of the chlorosome (Figure 7AS, middle right, Supporting Information). The density of the lowest and most other exciton states of the rod assembly was smoothly distributed around the circumference of the *B* rod (Figure 7AS, middle left, Supporting Information). For spiral systems, the exciton densities of the absorbing state became delocalized in a similar way as in the rod assembly. The lowest exciton state of an ideal Archimedean spiral antenna assembly poses a special feature in having the density almost entirely on the innermost pigment arrays; the density for "smooth" spiral assembly roughly resembled that of the rod assembly (Figures 7BS−7CS in the Supporting Information).

According to the results presented so far, tubular antenna elements *A* and *B* absorb light approximately in the same wavelength region. From *A* antenna interacting with its four *B* rod neighbors, excitation energy will preferentially flow to the lowest exciton state of the *A* antenna that is isoenergetic with the absorbing state of the *B* antenna (Tables 7AS, 7BS, 8AS, and 8BS in the Supporting Information). *Under such energetic conditions, efficient EET from an A antenna to the surrounding B antenna in the direction perpendicular to the chlorosome main axis becomes energetically possible.* Excitation energy is first transferred from the delocalized absorbing state of the *A* rod to its localized lowest exciton state of the *A* rod and then to the isoenergetic and delocalized absorbing state of the *B* rod assembly.

Simulations for the *C* tubular antenna (rod and "smooth" spiral) interacting with four *B* antenna were done in a similar way as the simulations for the *A* antenna. In these simulations, in addition to varying the *C*−4*B* distance, the distance between the *C* antenna and the plane of the baseplate was varied, both in the range from 1.0 to 5.0 nm. The diagonal elements and orientations of the transition moments of the Bchl *c*'s in a single array facing the baseplate were also varied. The numerical results of these simulations are given in Tables 9AS−9DS in the Supporting Information. Graphical presentations of the exciton densities of the absorbing and lowest energy states are shown in the bottom images of Figures 7AS−7CS in the Supporting Information. In Table 9AS in the Supporting Information, the effects of various simulation parameters became most clearly visible for the 4*B* rod−*C* rod−baseplate system with 12 nm rod length. Reducing the *C*−4*B* distance and the distance between the *C* antenna and the baseplate from 5.0 to 1.0 nm induced a blue-shift of the absorbing state by 112 cm^{-1} with a concomitant lowering of the energy of the lowest exciton state by about 130 cm^{-1} with respect to the reference state. Changing the value of the diagonal elements in a single array of Bchl *c*'s facing the baseplate from 667 to 670 nm at $R(C-4B) = R'(C-\text{baseplate}) = 2.0$ nm distances shifted the energy of the lowest exciton state 106 cm^{-1} below the reference level. By changing the value of the orientation of the transition moment from 20 to 5°, an additional shift of 50 cm^{-1} was created. Lowering of the energy of the lowest exciton state results in localization of exciton density on the pigments of the *C* tubule facing the baseplate, while the density of the absorbing state is delocalized roughly on the pigments facing the *B*-tubules (Figures 7AS−7CS, bottom images, Supporting Information). For the long tubules, the effects are relatively smaller. In summary, both *B* and *C* rods absorb in the same spectral region, but with lowered diagonal energies in a single array of Bchl's of the *C* rod, the lowest exciton state of the *C*−4*B* assembly was slightly below the energy of the corresponding state of the *B*−6*B* rod assembly, allowing downhill EET from the *B* rod assembly to the *C* rod assembly toward the baseplate.

With hypothetical parallel lamella type pigment organization in chlosomes with 2.0 nm inter-lamella spacing, some 20−50 lamellae can be fitted in a typical chlorosome. There are two types of environments of the lamella elements in the chlorosome, the outermost lamellae next to the chlorosome envelope and the "bulk" lamellae. The bulk lamellae have identical neighbors. Structural models so far presented[19] imply that one side of a lamella is next to the chlorosome envelope (pigments at *A* position, Figure 8) and the other side next to the baseplate (pigments at *C* position, Figure 8) with the long axis of the lamella parallel to the long axis of the chlorosome.

dx.doi.org/10.1021/jp4011394 | J. Phys. Chem. B XXXX, XXX, XXX−XXX

Reducing the values of the diagonal elements of the exciton matrix of the lamella next to the envelope from the non-perturbed value of $\lambda^* = 667$ resulted in lowering of the energy of the lowest exciton state and EET from the bulk lamella to the outermost lamella would be favored. On the other hand, if the lamella−lamella interaction was strong (Tables 5ES and 5FS in the Supporting Information) and/or the lamella−envelope interaction increased the monomeric Q_y transition energy (all diagonal elements blue-shifted) or decreased the absolute value of the monomeric Q_y transition dipole vector, the lowest exciton state of the outermost lamella was above the lowest exciton state of the bulk lamella. Then, excitation energy would be transferred from the outermost lamellae to the lowest exciton state of the bulk lamellae. To describe energy transfer from bulk lamellae to the baseplate, monomeric Q_y transition energies (Tables 1ES and 1FS in the Supporting Information) and the absolute value of the monomeric Q_y transition dipoles (Tables 2ES and 2FS in the Supporting Information) were varied in the outermost *A* and *C* pigment arrays of the lamellae. If the diagonal elements of the *C* array of the bulk lamella next to the baseplate were red-shifted to $\lambda^* = 675$ nm or μ^* increased by 25% and *A* pigments left non-perturbed, then localization of the lowest exciton state on the *C* pigments of the lamella took place (Figure 3CS in the Supporting Information) and efficient energy transfer from bulk lamella to the baseplate complex became possible.

4.7. Intra-Chlorosome and from Chlorosome to Baseplate Excitation Energy Transfer Time Constants. Chlorosome to baseplate excitation energy transfer rates were evaluated for several pigment organizations in the chlorosome and for two model baseplates. The following parameters were used: antenna length of 101.7 nm (71.1 nm for spirals and multiwall rods), inter-antenna distance in the antenna stack of 2.0 nm, and *C* antenna−baseplate distances of 3.0 and 5.0 nm. Orientations of monomeric transition dipole vectors of antenna elements were set to $\phi = 85°$ and $\theta = 20°$. Rate calculations were performed with $\lambda^* = 670$ nm and without $\lambda^* = 667$ nm environmental interactions for the *C* antennae. *A*-type antenna elements were not perturbed. For monomeric and dimeric structures of the 2D baseplate, $\lambda^* = 792$ nm for all Bchl *a*'s was used. The entire stacked antenna complex was positioned on top and in the center of the baseplate lattice. The energy gap between the lowest exciton states of the *C* antenna and the baseplate turned out to be about 300−500 cm^{-1}. To make resonance energy transfer from the *C* antenna to the baseplate possible, the homogeneous width of the excitonic states of the baseplates was set to 800 cm^{-1} to account for vibronic broadening. For the vibronic transitions, a Franck−Condon (FC) factor of 0.005 was used. The results of EET time constant calculations are given in Figures 8AS−8CS in the Supporting Information.

For all modeled antenna elements studied, intra-antenna excitation relaxation, i.e., relaxation from the main absorbing state of the antenna element to the lowest exciton state of the antenna, occurred faster than 100 fs. The dominant time constants from *A* rod to *B* rods and from *B* rod to *B* rods were estimated to be 235 and 250 fs, respectively. EET from *B* rod to *C* rod was also very fast 253 fs, but it was accompanied by slower times of 3.2 and 23 ps with smaller amplitudes (Figure 8AS, Supporting Information). For non-interacting rods, which have delocalized lowest exciton states, the sub-ps time components became about 2 times slower with clearly smaller amplitude and the few ps (3−5 ps) component gained in amplitude.

EET time constants from *C* rods to the dimeric baseplate (dBP) at a rod−baseplate distance of 3.0 nm and $\lambda^* = 667$ nm were 5.4 ps (0.44), 22 ps (0.33), and 103 ps (0.23). At longer *C* rod−dBP distance of 5.0 nm, the time constants became longer by a factor of 3−4 (Figure 8AS in the Supporting Information). Perturbation of the Bchl *c* array of the *C* rod on the baseplate side ($\lambda^* = 670$ nm) had only a marginal effect on the time constants (Figure 8AS in the Supporting Information). EET from *C* rods to monomeric baseplate (mBP) in general turned out to be slightly faster than EET from *C* rods to dBP (Figure 8AS in the Supporting Information).

In isolated concentric double wall rods with a wall separation of 2.0 nm, a very fast intra-antenna EET process from the absorbing exciton state of the inner tube to the outer tube was identified with a dominant time component of 25 fs and two additional components of 190 fs and 4.5 ps with much lower amplitudes. Interestingly, for the stacked double wall rod antenna, inter-antenna and antenna−baseplate EET times were only slightly slower than the corresponding time constants for stacked single wall rods.

For parallel lamella organization of the pigments in the chlorosome at an inter-lamella distance of 2.0 nm, extremely fast inter-lamellae EET time constants of 60 fs (0.27) and 835 fs (0.54) and minor component 3.3 ps (0.19) were estimated (Figure 8BS in the Supporting Information), with EET being almost by a factor of 4 faster as compared to stacked tubular antenna at the same inter-antenna separation. At a distance of 3.0 nm between lamellae and dBP with non-perturbed *C* pigments of the lamellae, the EET time constant became 5.2 ps (0.23), 27 ps (0.37), and 368 ps (0.40). Transfer times to mBP were almost by a factor of 3 faster (Figure 8BS in the Supporting Information).

For "smooth" spiral antenna stacks, time constants of about 530 fs (0.48), 6.3 ps (0.39), and 48 ps (0.13) for EET from *A* to *C* spiral were obtained (Figure 8CS in the Supporting Information). From *C* type spiral to dBP with perturbations on pigments facing the BP, the EET time constants were 4.1 ps (0.59), 16 ps (0.28), and 127 ps (0.13) and somewhat slower for the non-perturbed *C* pigments. Excitation transfer from *C* spirals to monomeric baseplate was 3 times faster than that to dimeric baseplate (Figure 8CS in the Supporting Information). For ideal Archimedean spirals, intra-antenna and antenna−baseplate rates were typically in the range 10−100 ps for the reason of accumulation of the exciton density almost entirely to the innermost pigment arrays of the spiral forming the lowest energy state.

5. DISCUSSION

5.1. Environmental Effects on Exciton Energies. One of the interesting results of the present work is that the energy gap between the main absorption band and the lowest excited state (optically forbidden) increases significantly, when Q_y transition energies of the pigments in a single array of an antenna are reduced and/or antennae become close to each other. Much weaker effects are observed when pigments in the end(s) of the antenna are perturbed (Table 1S in the Supporting Information). Calculated energy gap values for all antenna elements studied fall in an energy domain of 170−450 cm^{-1} reported in several hole-burning studies.[15,78,82,83]

Both the magnitude and orientation of the monomeric Q_y transition dipole vectors have an impact on spectroscopic and

dx.doi.org/10.1021/jp4011394 | J. Phys. Chem. B XXXX, XXX, XXX−XXX

EET properties of the antenna elements. Changes in these parameters have the strongest consequences for couplings in linear pigment arrays of the antenna but weaker effects on pigments on the edges of the antenna elements (Tables 2S−4S in the Supporting Information). Increasing the absolute value of the Q_y transition dipole or decreasing the orientation angle θ on a single array of pigments increases exciton couplings between these pigments in the antenna, red-shifts and localizes the lowest exciton state, but does not have much effect on the main absorbing state (Tables 2S and 3S in the Supporting Information). Because the inter-array exciton interactions are weak, changes in the second orientation angle ϕ do not induce significant effects (Table 4S in the Supporting Information).

High-resolution EM images show that chlorosomes contain a small fraction of lamellar aggregates. Excitation energy may flow also between lamellar and tubular antenna elements. The direction of the flow is dependent on the relative sizes and orientations of the lamella (width and length) and the tubular antenna.[52] If both antenna elements have identical pigment architectures (same θ, ϕ, and inter-pigment distance), downhill energy transfer from a tube parallel to a large lamella is possible. If the pigments of the lamellae organize into narrow stripes (short or long), energy transfer from the lamella to a parallel rod or a spiral is also possible.[52] In a hypothetical lamellar organization of pigments, the chlorosome baseplate−lamella interaction has to be stronger than the envelope−lamella interaction to make excitation energy transfer toward the baseplate possible.

5.2. Localization of Exciton Density and Energy Transfer. The exciton area of the lowest excited state of an antenna element turned out to be strongly dependent on monomeric transition energies and transition dipole vectors of the pigments of the antenna (see Tables 1S−5S and Figures 3AS−3CS in the Supporting Information). The exciton density of the lowest exciton state of the antenna becomes localized on the perturbed Bchl's if perturbed pigments have lower transition energies or higher absolute values of transition dipoles than the rest of the pigments of the antenna. On the contrary, the lowest exciton state is delocalized over the entire antenna surface if the transition energies are higher or the transition moments are lower on the perturbed Bchl's than in the rest of the Bchl's of the antenna. Localization of the lowest exciton state takes place also due to interactions of two or more antenna elements at inter-antenna distances of about 2.0 nm (see Figures 5AS−5FS in the Supporting Information), and the density of the lowest exciton state of the antenna is localized in the region(s) facing the neighboring antennae. Higher excitonic states are in general delocalized over the entire antennae. A few high exciton states show localization around "high energy pigments".

Antenna elements in the chlorosomal vesicle were grouped in three categories, antenna next to the chlorosome envelope (*A*), "bulk" antenna (*B*), and antenna next to the baseplate (*C*). It was shown that local environmental perturbations provide efficient excitation energy transfer from a tubular (single or multiwalled rod or slowly winding spiral) *A* antenna via *B* antennae to *C* antennae and finally to Bchl *a*'s of the baseplate. The lowest exciton state of a tubular *A* antenna element is localized in the region of the antenna facing the neighboring *A* or *B* antenna. The delocalized absorbing state of the *B* antenna is almost isoenergetic with the lowest exciton state of the *A* antenna which allows resonance EET from *A* to *B* antenna to proceed (see Figures 7AS−7DS and 8AS−8DS in the Supporting Information). The environment of the *B* type antenna is nearly homogeneous, and thus, exciton states of these antenna elements are almost delocalized, though the density of the lowest exciton state is preferentially localized toward the neighboring *B* antenna. Excitation energy transfer between *B* antenna elements is possible via resonance energy transfer. The same is true also between the *B* and *C* antennae. An environment induced red-shift of the lowest exciton state of the *C* antenna or vibronic contributions are needed to make EET from *B* antenna toward the *C* antenna to take place.

The excitation energy transfer mechanisms described above are probably functional also in membranes of purple photosynthetic bacteria, where excitons have to travel over several circular LH2 antennae to the LH1−RC complex. Antenna−antenna interactions between membrane bound light harvesting antennae (LH2) localize exciton density on pigments of the initially excited B850 ring (or B820 ring) facing the pigments of the B850 (or B820) ring of the next LH2 complex. Environmental effects around the last LH2 antenna before the LH1−RC complex determine the efficiency of excitation transfer to the reaction center. Local protein−pigment interactions around chlorophylls of peripheral light harvesting-II (LHC-II) antenna also localize exciton density on a single monomer unit of trimeric LHC-II facing a photosystem II (PSII) complex,[84] allowing effective EET from the LHC-II to the accessory Chl complexes and to the RC of the PSII.[52]

Calculated excitation energy transfer time constants between antenna elements depend mainly on inter-antenna distances. The calculated EET time constants of about 235−250 fs between tubular antenna elements at an inter-rod distance of about 2.0 nm are similar to experimentally recorded time constants of 200−500 fs for chlorosomes of FAP and GSB.[35,37,38] The calculated inter-lamella EET is about an order of magnitude faster than experimentally observed intra-chlorosome EET. The presence of lamellar aggregates as a minor species in the chlorosome according to the present results is fully possible and would only have a minor influence on the chlorosome EET time constants. For all antenna elements studied, 5−20 ps antenna−baseplate EET time constants were obtained, which is also in good agreement with experimental observations.[37,38] Present results may be compared to well documented EET time constants obtained for light harvesting antennae of purple bacteria, for which inter-ring distances are known precisely. EET time constants from B800 to B850 antenna with an inter-antenna distance of about 1.8 nm have been determined to be 700 fs at RT,[80,85] which is in the same range as the calculated time constants for the tubular antenna stack modeled in the present paper at 2.0 nm inter-antenna distance.

The influence of the thermal population of the exciton states on the EET rate constants in photosynthetic light harvesting has been previously addressed for the LH2 antennae of *Rbs. sphaeroides*[86] and for the PSU of *Rps. acidophila*.[87] In the calculation of the EET rate constants from eq 14, such temperature effects were not included. In the former simulation,[86] it was assumed that the time scale of intra-B850 ring thermal relaxation is much faster than the inter-B850 ring excitation transfer. Authors then concluded that EET between the B850 rings occurs from Boltzmann-weighted intra-ring exciton states. They treated both intra- and inter-antenna processes in their model non-perturbatively in the framework of generalized Förster theory to obtain the final conclusion that in practice five lowest exciton states are responsible for inter-B850

dx.doi.org/10.1021/jp4011394 | J. Phys. Chem. B XXXX, XXX, XXX−XXX

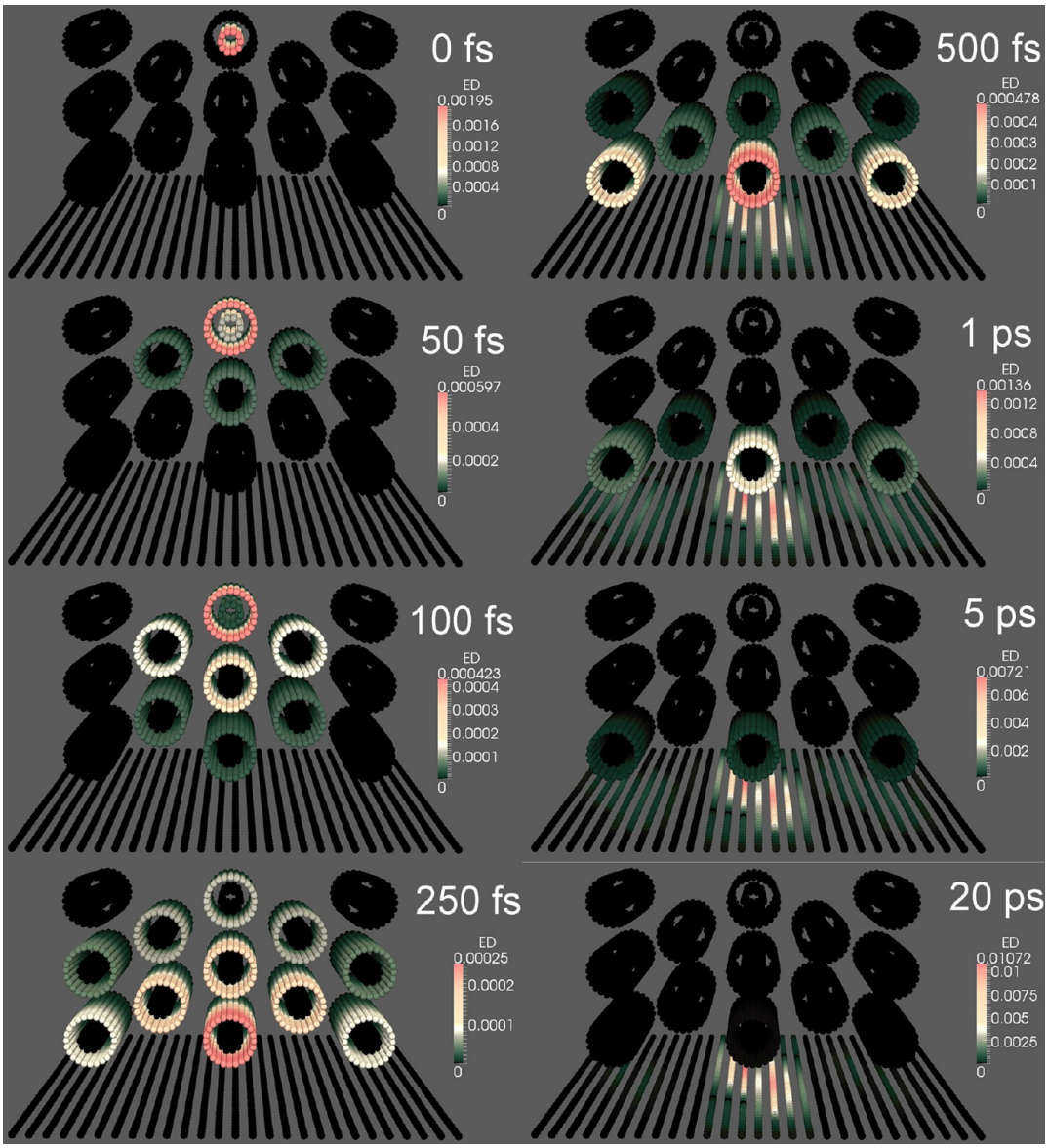

Figure 11. Spatial and temporal visualization of advancement of exciton density from chlorosome to the baseplate for a double wall rod-like Bchl *c* antenna system and a baseplate consisting of a 2D lattice of dimeric Bchl *a* molecules. On the top right corner of each image, elapsed time after excitation is shown; below the time marks, color-coding for exciton densities is given. The following simulation parameters were used: antenna length of 101.7 nm, rod antenna inner wall diameter of 2.9 nm, rod antenna outer wall diameter of 6.9 nm, inter-rod distance of 2 nm, antenna−dBP distance of 3 nm, diagonal matrix elements $\lambda^* = 667$ nm ($\lambda^* = 670$ nm for Bchl *c*'s of *C* type rods and $\lambda = 792$ nm for Bchl *a*'s), $\phi = 85°$ and $\theta = 20°$ (80 and 100° for Bchl *a*'s).

ring EET. Only two interacting B850 rings were considered.[86] In the latter simulation,[87] a vibronic exciton Hamiltonian containing linear exciton−phonon coupling was used to evaluate the EET rate constants of the PSU of *Rps. acidophila*.[87] This simulation included among other things calculation of the vibrational levels of the LH2 antenna complex and simulation of the temperature dependence of the Bchl *a*−B800 absorption spectrum. Temperature dependences of the rate constants from Bchl *a*−B800 to Bchl *a*−B850 ring were evaluated being 0.6 ps at RT and 1.6 ps at 4 K. Both approaches[86,87] did produce intra- and inter-antenna EET rate constants, that were comparable to the experimentally recorded rate constants. In both cases, also accurate atomic coordinates of the complexes were available, which is a prerequisite for testing of the more advance theories.

In simulation of large pigment systems, such as antenna elements of chlorosomes, use of more advanced approaches than those used in the present study may be questioned. First of all, the structures generated at the molecular mechanics level of calculation are just first order models for real antenna structures in chlorosomes. Second, correct inclusion of Boltzmann distributions would require knowledge of vibrational states and assumptions on Franck−Condon factors of the modeled antennae if the approach we used for the PSU of *Rps. acidophila* had been adopted.[87] Calculation of vibrational eigenvalues for an antenna element containing hundreds of Bchl *c*'s with more than 140 atoms is not practical. It is also not feasible to consider the modeled antenna as quantum systems and try to derive equations of motions describing the quantum dynamics of the system, as can be done in the case of two interacting B850 rings.[86]

dx.doi.org/10.1021/jp4011394 | *J. Phys. Chem. B* XXXX, XXX, XXX−XXX

We only can qualitatively discuss the effects of thermal excitations in the antenna and antenna assemblies. Relaxation from thermally populated exciton states would slow down the depopulation of the initially prepared state, and hence, rate constants calculated from eq 14 would represent upper limits. The thermal population cannot cause an order of magnitude effect, as seen from the temperature dependencies of the rate constants calculated from Bchl *a*−B800 to Bchl *a*−B850 EET for LH2 antenna.[87] In chlorosome antenna assemblies like *A*(*C*)−4*B* or *B*−6*B*, thermally populated delocalized exciton states of the initially excited antenna would be prone, besides internal relaxation, to EET to iso-energetic delocalized exciton states of the neighboring antenna. With neighbors, relaxation of the thermally excited states of *A* or *B* antennae would then compete with four or six EET channels from the thermally excited states *A* or *B* to the exciton states of the neighboring antenna, respectively, and hence, relaxation to the initial state would be diminished. To estimate quantitatively the proportion of thermal relaxation would be a difficult task, but due to packing and size of the antenna elements in chlorosomes, there are always EET channels available, for an excited antenna, also from thermally populated states, to transfer its excitation to neighboring antenna. Thermal effects are probably more pronounced in dimeric ring systems, where only one such EET channel is available and the density of exciton states much lower than in chlorosomal antennae.[86]

5.3. Spatial and Temporal Advancement of Excitation from Chlorosome to Baseplate. The main goal of this work was to establish a spatial and temporal model for advancement of excitation in the chlorosomes and from chlorosome to the baseplate. The rate constant presented above can be used to do excitation energy transfer population analysis in space and time both for intra-chlorosomal and for from chlorosome to baseplate EET by using equations 14−19.

Spatial visualization of intra-chlorosomal EET was performed for a model that consisted of stacked double rod antenna elements, which is a reasonable model for pigment organization in the chlorosomes of GSB. In Figure 11, spatial and temporal advancement of exciton density from the initially excited inner surface of an *A* type Bchl *c* double wall rod to a 2D lattice of monomeric Bchl *a* molecules is presented. Excitation landing on the inner surface of an *A* rod after reaching the outer surface in 50 fs spreads to three neighboring *B* rods in about 100 fs and continues advancing toward further five *B* and three *C* rods in about 250 fs. Excitation is finally delivered to the baseplate from the three *C* type rods and arrives to the baseplate between 5 and 20 ps after excitation. According to the simulation, the majority of intra-chlorosomal EET is over in less than 1 ps. As mentioned already above, the calculated time constants for intra-chlorosome and chlorosome to baseplate are in nice agreement with the experimental EET time constants of 300 fs to 1 ps and 8 to 12 ps reported for chlorosomes of GSB, respectively.[38]

Chlorosomes of FAP that are believed to contain stacked single wall rods, an intra-chlorosomal EET time of 200−300 fs and from chlorosome to baseplate of 6.6−9.2 ps has been observed experimentally.[35,37,38] These time constants also match the simulated temporal EET evolution shown in Figure 11. In chlorosomes containing stacked multiwalled rods, the EET mechanism is similar to that for the double wall rods with the difference that the major absorbing state in the multiwalled rods is the tubular pigment layer next to the outermost pigment layer. In multiwall antenna elements, the EET from the absorbing state to the outermost pigment surface is as fast as the initial transfer from the inner to outer wall in double wall tubes. In chlorosomes that contain mixtures of tubular and lamellar antenna elements, the EET efficiency depends on the concentration, orientations, and sizes of these minority antenna.

CONCLUSIONS

The results of the present paper suggest that excitation energy transfer (EET) in chlorosomes is driven by environmental interactions that localize exciton wave functions of tubular antenna elements. It was shown that stacked tubular antenna elements in different chlorosome environments, near the chlorosome envelope, in the bulk and near the baseplate may form an excitonic light harvesting unit with a built in energy gradient that drives intra-chlorosome and from chlorosome to baseplate EET in the perpendicular direction to the main symmetry axis of the chlorosome. Calculated time constants for intra-chlorosome and from chlorosome to baseplate EET in stacked tubular antenna elements of from 200 to 500 fs and from 5 to 20 ps, respectively, are in good agreement with experimental results reported for isolated chlorosomes from FAP and GSB. Spatial and temporal advancement of intra-chlorosomal and chlorosome to baseplate excitation energy transfer in a double wall rod antenna assembly, mimicking pigment organization in the chlorosomes of GSB, was visualized.

ASSOCIATED CONTENT

Supporting Information

Two supporting documents that are closely related to this paper have been prepared. One of the documents (jp4011394_si_001.pdf) contains supplementary figures: energy levels for multiwalled rod antenna and large spirals, color coded 2D exciton densities of antenna elements and antenna element dimers, calculated absorption, LD and CD spectra, and exponential fits to the calculated EET rate constant distributions. The other document (jp4011394_si_002.pdf) contains detailed numerical results for calculated energy level shifts of the absorbing states and the lowest exciton states and relative exciton areas of the lowest exciton states of the perturbed antenna elements as well as of interacting antennae. This material is available free of charge via the Internet at http://pubs.acs.org.

AUTHOR INFORMATION

Corresponding Author

*E-mail: ktommola@jyu.fi.

Notes

The authors declare no competing financial interest.

ACKNOWLEDGMENTS

Financial support from the Academy of Finland is greatly appreciated (Contract No. 123801). J.M.L. gratefully acknowledges a grant from Magnus Ehrnrooth Foundation and grant MJD262 from the Estonian Research Council. The authors gratefully acknowledge Jyrki Hokkanen from IT Center for Science, CSC, Finland, for 3D graphics presented in this paper.

REFERENCES

(1) Cohen-Bazire, G.; Pfenning, N.; Kunisawa, R. The Fine Structure of Green Bacteria. *J. Cell Biol.* **1964**, *22*, 207−225.

(2) Bryant, D. A.; Costas, A. M. G.; Maresca, J. A.; Chew, A. G. M.; Klatt, C. G.; Bateson, M. M.; Tallon, L. J.; Hostetler, J.; Nelson, W. C.; Heidelberg, J. F.; Ward, D. M. Candidatus Chloracidobacterium thermophilum: An Aerobic Phototrophic Acidobacterium. *Science* **2007**, *317*, 523−526.
(3) Cruden, D. L.; Stanier, R. Y. The Characterization of Chlorobium Vesicles and Membranes Isolated from Green Bacteria. *Arch. Microbiol.* **1970**, *72*, 115−134.
(4) Staehelin, L. A.; Golecki, J. R.; Drews, G. Supramolecular Organization of Chlorosomes (Chlorobium Vesicles) and of Their Membrane Attachment Sites in Chlorobium limicola. *Biochim. Biophys. Acta* **1980**, *589*, 30−45.
(5) Feick, R. G.; Fuller, R. C. Topography of the Photosynthetic Apparatus of Chloroflexus aurantiacus. *Biochemistry* **1984**, *23*, 3693−3700.
(6) Golecki, J. R.; Oelze, J. Quantitative Relationship between Bacteriochlorophyll Content, Cytoplasmic Membrane Structure and Chlorosome Size in *Chloroflexus aurantiacus*. *Arch. Microbiol.* **1987**, *148*, 236−241.
(7) Oelze, J.; Golecki, J. R. In *Anoxygenic Photosynthetic Bacteria*; Blankenship, R. E., Madigan, M. T., Bauer, C. E., Eds.; Kluwer Academic Publishers: Dordrecht, The Netherlands, 1995; p 259.
(8) Zhu, Y.; Ramakrishna, B. L.; van Noort, P. I.; Blankenship, R. E. Microscopic and Spectroscopic Studies of Untreated and Hexanol-Treated Chlorosomes from Chloroflexus aurantiacus. *Biochim. Biophys. Acta* **1995**, *1232*, 197−207.
(9) Foidl, M.; Golecki, J. R.; Oelze, J. Chlorosome Development in Chloroflexus aurantiacus. *Photosynth. Res.* **1998**, *55*, 109−114.
(10) Olson, J. M. Chlorophyll Organization and Function in Green Photosynthetic Bacteria. *Photochem. Photobiol.* **1998**, *67*, 61−75.
(11) Martinez-Planells, A.; Arellano, J. B.; Borrego, C. M.; Garcia-Gil, J.; Gich, F. Determination of the Topography and Biometry of Chlorosomes by Atomic Force Microscopy. *Photosynth. Res.* **2002**, *71*, 83−90.
(12) Taisova, A. S.; Keppen, O.I.; Lukashev, E. P.; Arutyunyan, A. M.; Fetisova, Z. G. Study of the Chlorosomal Antenna of the Green Mesophilic Filamentous Bacterium Oscillochloris trichoides. *Photosynth. Res.* **2002**, *74*, 73−85.
(13) Vassilieva, E. V.; Stirewalt, V. L.; Jakobs, C. U.; Frigaard, N.-U.; Inoue-Sakamoto, K.; Baker, M. A.; Sotak, A.; Bryant, D. A. Subcellular Localization of Chlorosome Proteins in Chlorobium tepidum and Characterization of Three New Chlorosome Proteins: CsmF, CsmH, and CsmX. *Biochemistry* **2002**, *41*, 4358−4370.
(14) Montaño, G. A.; Bowen, B. P.; LaBelle, J. T.; Woodbury, N. W.; Pizziconi, V. B.; Blankenship, R. E. Characterization of Chlorobium tepidum Chlorosomes: A Calculation of Bacteriochlorophyll c per Chlorosome and Oligomer Modeling. *Biophys. J.* **2003**, *85*, 2560−2565.
(15) Fetisova, Z. G.; Mauring, K. Experimental Evidence of Oligomeric Organization of Antenna Bacteriochlorophyll c in Green Bacterium Chloroflexus aurantiacus by Spectral Hole Burning. *FEBS Lett.* **1992**, *307*, 371−374.
(16) Montaño, G. A.; Wu, H.-L.; Lin, S.; Brune, D. C.; Blankenship, R. E. Isolation and Characterization of the B798 Light-Harvesting Baseplate from the Chlorosomes of Chloroflexus aurantiacus. *Biochemistry* **2003**, *42*, 10246−10251.
(17) Staehelin, L. A.; Golecki, J. R.; Fuller, R. C.; Drews, G. Visualization of the Supramolecular Architecture of Chlorosomes (Chlorobium Type Vesicles) in Freeze-Fractured Cells of Chloroflexus aurantiacus. *Arch. Microbiol.* **1978**, *119*, 269−277.
(18) Saga, Y.; Tamiaki, H. Transmission Electron Microscopic Study on Supramolecular Nanostructures of Bacteriochlorophyll Self-Aggregates in Chlorosomes of Green Photosynthetic Bacteria. *J. Biosci. Bioeng.* **2006**, *102*, 118−123.
(19) Psencík, J.; Ikonen, T. P.; Laurinmäki, P.; Merckel, M. C.; Butcher, S. J.; Serimaa, R. E.; Tuma, R. Lamellar Organization of Pigments in Chlorosomes, the Light Harvesting Complexes of Green Photosynthetic Bacteria. *Biophys. J.* **2004**, *87*, 1165−1172.
(20) Psencík, J.; Arellano, J. B.; Ikonen, T. P.; Borrego, C. M.; Laurinmäki, P. A.; Butcher, S. J.; Serimaa, R. E.; Tuma, R. Internal Structure of Chlorosomes from Brown-Colored Chlorobium Species and the Role of Carotenoids in Their Assembly. *Biophys. J.* **2006**, *91*, 1433−1440.
(21) Oostergetel, G. T.; Reus, M.; Chew, A. G. M.; Bryant, D. A.; Boekema, E. J.; Holzwarth, A. R. Long-Range Organization of Bacteriochlorophyll in Chlorosomes of Chlorobium tepidum Investigated by Cryo-Electron Microscopy. *FEBS Lett.* **2007**, *581*, 5435−5439.
(22) Oostergetel, G. T.; van Amerongen, H.; Boekema, E. J. The Chlorosome: A Prototype for Efficient Light Harvesting in Photosynthesis. *Photosynth. Res.* **2010**, *104*, 245−255.
(23) Hohmann-Marriott, M. F.; Blankenship, R. E.; Roberson, R. W. The Ultrastructure of Chlorobium tepidum Chlorosomes Revealed by Electron Microscopy. *Photosynth. Res.* **2005**, *86*, 145−154.
(24) Psencik, J.; Torkkeli, M.; Zupcanova, A.; Vacha, F.; Serimaa, R. E.; Tuma, R. The Lamellar Spacing in Self-Assembling Bacteriochlorophyll Aggregates Is Proportional to the Length of the Esterifying Alcohol. *Photosynth. Res.* **2010**, *104*, 211−219.
(25) Ganapathy, S.; Oostergetel, G. T.; Wawrzyniak, P. K.; Reus, M.; Chew, A. G. M.; Buda, F.; Boekema, E. J.; Bryant, D. A.; Holzwarth, A. R.; de Groot, H. J. M. Alternating Syn-Anti Bacteriochlorophylls Form Concentric Helical Nanotubes in Chlorosomes. *Proc. Natl. Acad. Sci. U.S.A.* **2009**, *106*, 8525−8530.
(26) Shoji, S.; Hashishin, T.; Tamiaki, H. Construction of Chlorosomal Rod Self-Aggregates in the Solid State on Any Substrates from Synthetic Chlorophyll Derivatives Possessing an Oligomethylene Chain at the 17-Propionate Residue. *Chem.—Eur. J.* **2012**, *18*, 13331−13341.
(27) Pedersen, M. Ø.; Pham, L.; Steensgaard, D. B.; Miller, M. A Reconstituted Light-Harvesting Complex from the Green Sulfur Bacterium Chlorobium tepidum Containing CsmA and Bacteriochlorophyll a. *Biochemistry* **2008**, *47*, 1435−1441.
(28) van Dorssen, R. J.; Vasmel, H.; Amesz, J. Pigment Organization and Energy Transfer in the Green Photosynthetic Bacterium Chloroflexus aurantiacus II. The Chlorosome. *Photosynth. Res.* **1986**, *9*, 33−45.
(29) Matsuura, K.; Hirota, M.; Shimada, K.; Mimuro, M. Spectral Forms and Orientation of Bacteriochlorophylls c and α in Chlorosomes of the Green Photosynthetic Bacterium Chloroflexus aurantiacus. *Photochem. Photobiol.* **1993**, *57*, 92−97.
(30) Pedersen, M. Ø.; Linnanto, J.; Frigaard, N.-U.; Nielsen, N. C.; Miller, M. A Model of the Protein−Pigment Baseplate Complex in Chlorosomes of Photosynthetic Green Bacteria. *Photosynth. Res.* **2010**, *104*, 233−243.
(31) Savikhin, S.; Zhu, Y.; Lin, S.; Blankenship, R. E.; Struve, W. S. Femtosecond Spectroscopy of Chlorosome Antennas from the Green Photosynthetic Bacterium Chloroflexus aurantiucus. *J. Phys. Chem.* **1994**, *98*, 10322−10334.
(32) Savikhin, S.; Zhu, Y.; Blankenship, R. E.; Struve, W. S. Ultrafast Energy Transfer in Chlorosomes from the Green Photosynthetic Bacterium Chloroflexus aurantiacus. *J. Phys. Chem.* **1996**, *100*, 3320−3322.
(33) Savikhin, S.; van Noort, P. I.; Zhu, Y.; Lin, S.; Blankenship, R. E.; Struve, W. S. Ultrafast Energy Transfer in Light-Harvesting Chlorosomes From the Green Sulfur Bacterium Chlorobium tepidum. *Chem. Phys.* **1995**, *194*, 245−258.
(34) Psencik, J.; Polívka, T.; Nemec, P.; Dian, J.; Kudrna, J.; Maly, P.; Hala, J. Fast Energy Transfer and Exciton Dynamics in Chlorosomes of the Green Sulfur Bacterium Chlorobium tepidum. *J. Phys. Chem. A* **1998**, *102*, 4392−4398.
(35) Psencík, J.; Ma, Y.-Z.; Arellano, J. B.; Hála, J.; Gillbro, T. Excitation Energy Transfer Dynamics and Excited-State Structure in Chlorosomes of Chlorobium phaeobacteroides. *Biophys. J.* **2003**, *84*, 1161−1179.
(36) Steensgaard, D. B.; van Walree, C. A.; Permentier, H.; Borrego, C. M.; Garcia-Gil, J.; Aartsma, T. J.; Amesz, J.; Holzwarth, A. R. Fast Energy Transfer between BChl d and BChl c in Chlorosomes of the

Green Sulfur Bacterium Chlorobium limicola. *Biochim. Biophys. Acta* **2000**, *1457*, 71−80.
(37) Martiskainen, J.; Linnanto, J.; Kananavicius, R.; Lehtovuori, V.; Korppi-Tommola, J. Excitation Energy Transfer in Isolated Chlorosomes from Chloroflexus aurantiacus. *Chem. Phys. Lett.* **2009**, *477*, 216−220.
(38) Martiskainen, J.; Linnanto, J.; Aumanen, V.; Myllyperkiö, P.; Korppi-Tommola, J. Excitation Energy Transfer in Isolated Chlorosomes from Chlorobaculum tepidum and Prosthecochloris aestuarii. *Photochem. Photobiol.* **2012**, *88*, 675−683.
(39) Dostál, J.; Mančal, T.; Augulis, R.; Vácha, F.; Pšenčík, J.; Zigmantas, D. Two-Dimensional Electronic Spectroscopy Reveals Ultrafast Energy Diffusion in Chlorosomes. *J. Am. Chem. Soc.* **2012**, *134*, 11611−11617.
(40) Fetisova, Z.; Freiberg, A.; Novoderezhkin, V.; Taisova, A.; Timpmann, K. Antenna Size Dependent Exciton Dynamics in the Chlorosomal Antenna of the Green Bacterium Chloroflexus aurantiacus. *FEBS Lett.* **1996**, *383*, 233−236.
(41) Ma, Y.-Z.; Cox, R. P.; Gillbro, T.; Miller, M. Bacteriochlorophyll Organization and Energy Transfer Kinetics in Chlorosomes from Chloroflexus aurantiacus Depend on the Light Regime during Growth. *Photosynth. Res.* **1996**, *47*, 157−165.
(42) Timpmann, K. E.; Taisova, A. S.; Novoderezhkin, V. I.; Fetisova, Z. G. Functioning of Oligomeric-Type Light-Harvesting Antenna. *Biochem. Mol. Biol. Int.* **1997**, *42*, 21−27.
(43) Yakovlev, A. G.; Taisova, A. S.; Fetisova, Z. G. Light Control over the Size of an Antenna Unit Building Block as an Efficient Strategy for Light Harvesting in Photosynthesis. *FEBS Lett.* **2002**, *512*, 129−132.
(44) Causgrove, T. P.; Brune, D. C.; Blankenship, R. E. Förster Energy Transfer in Chlorosomes of Green Photosynthetic Bacteria. *J. Photochem. Photobiol., B* **1992**, *15*, 171−179.
(45) Novoderezhkin, V. I.; Fetisova, Z. G. Structure of Bacteriochlorophyll Aggregates in Chlorosomes of Green Bacteria: A Spectral Hole Burning Study. *Biochem. Mol. Biol. Int.* **1996**, *40*, 243−252.
(46) Mizoguchi, T.; Hara, K.; Nagae, H.; Koyama, Y. Structural Transformation among the Aggregate Forms of Bacteriochlorophyll c as Determined by Electronic-Absorption and NMR Spectroscopies: Dependence on the Stereoisomeric Configuration and on the Bulkiness of the 8-C Side Chain. *Photochem. Photobiol.* **2000**, *71*, 596−609.
(47) Prokhorenko, V. I.; Steensgaard, D. B.; Holzwarth, A. R. Exciton Dynamics in the Chlorosomal Antennae of the Green Bacteria Chloroflexus aurantiacus and Chlorobium tepidum. *Biophys. J.* **2000**, *79*, 2105−2120.
(48) Novoderezhkin, V.; Taisova, A.; Fetisova, Z. G. Unit Building Block of the Oligomeric Chlorosomal Antenna of the Green Photosynthetic Bacterium Chloroflexus aurantiacus: Modeling of Nonlinear Optical Spectra. *Chem. Phys. Lett.* **2001**, *335*, 234−240.
(49) Didraga, C.; Knoester, J. Absorption and Dichroism Spectra of Cylindrical J Aggregates and Chlorosomes of Green Bacteria. *J. Lumin.* **2003**, *102-103*, 60−66.
(50) Prokhorenko, V. I.; Steensgaard, D. B.; Holzwarth, A. R. Exciton Theory for Supramolecular Chlorosomal Aggregates: 1. Aggregate Size Dependence of the Linear Spectra. *Biophys. J.* **2003**, *85*, 3173−3186.
(51) Linnanto J.; Korppi-Tommola, J. A Theoretical Model for Excitation Energy Transfer in Chlorosomes: Lamellar and Rod-Shaped Antenna Structures. In *Photosynthesis. Energy from the Sun*; Allen, J. F., Gantt, E., Golbeck, J., Osmond, B., Eds.; Springer: Netherlands, 2007; p 287.
(52) Linnanto, J. M.; Korppi-Tommola, J. E. I. Investigation on Chlorosomal Antenna Geometries: Tube, Lamella and Spiral-Type Self-Aggregates. *Photosynth. Res.* **2008**, *96*, 227−245.
(53) Linnanto, J. M.; Korppi-Tommola, J. E. I. Modelling Excitonic Energy Transfer in the Photosynthetic Unit of Purple Bacteria. *Chem. Phys.* **2009**, *357*, 171−180.
(54) Pajusalu, M.; Rätsep, M.; Trinkunas, G.; Freiberg, A. Davydov Splitting of Excitons in Cyclic Bacteriochlorophyll a Nanoaggregates of Bacterial Light-Harvesting Complexes between 4.5 and 263 K. *ChemPhysChem* **2011**, *12*, 634−644.
(55) Gelzinis, A.; Abramavicius, D.; Valkunas, L. Non-Markovian Effects in Time-Resolved Fluorescence Spectrum of Molecular Aggregates: Tracing Polaron Formation. *Phys. Rev. B* **2011**, *84*, 245430.
(56) Linnanto, J.; Korppi-Tommola, J. E. I.; Helenius, V. M. Electronic States, Absorption Spectrum and Circular Dichroism Spectrum of the Photosynthetic Bacterial LH2 Antenna of *Rhodopseudomonas acidophila* as Predicted by Exciton Theory and Semiempirical Calculations. *J. Phys. Chem. B* **1999**, *103*, 8739−8750.
(57) Linnanto, J. M.; Korppi-Tommola, J. E. I. Excitation Energy-Transfer in the LH2 Antenna of Photosynthetic Purple Bacteria via Excitonic B800 and B850 States. *J. Chin. Chem. Soc.* **2000**, *47*, 657−665.
(58) Linnanto, J.; Korppi-Tommola, J. Quantum Chemical Simulation of Excited States of Chlorophylls, Bacteriochlorophylls and Their Complexes. *Phys. Chem. Chem. Phys.* **2006**, *8*, 663−687.
(59) Linnanto, J.; Martiskainen, J.; Lehtovuori, V.; Ihalainen, J.; Kananavicius, R.; Barbato, R.; Korppi-Tommola, J. Excitation Energy Transfer in the LHC-II Trimer: A Model Based on the New 2.72 A Structure. *Photosynth. Res.* **2006**, *87*, 267−279.
(60) Alden, R. G.; Lin, S. H.; Blankenship, R. E. Theory of Spectroscopy and Energy Transfer of Oligomeric Pigments in Chlorosome Antennas of Green Photosynthetic Bacteria. *J. Lumin.* **1992**, *51*, 51−66.
(61) Linnanto, J.; Korppi-Tommola, J. E. I. Theoretical Study of Excitation Transfer from Modified B800 Rings of the LH II Antenna Complex of Rps. acidophila. *Phys. Chem. Chem. Phys.* **2002**, *4*, 3453−3460.
(62) Linnanto, J.; Korppi-Tommola, J. Structural and Spectroscopic Properties of Mg-Bacteriochlorin and Methyl Bacteriochlorophyllides *a*, *b*, *g*, and *h* Studied by Semiempirical, ab Initio, and Density Functional Molecular Orbital Methods. *J. Phys. Chem. A* **2004**, *108*, 5872−5882.
(63) van Rossum, B.-J.; Steensgaard, D. B.; Mulder, F. M.; Boender, G. J.; Schaffner, K.; Holzwarth, A. R.; de Groot, H. J. M. A Refined Model of the Chlorosomal Antennae of the Green Bacterium Chlorobium tepidum from Proton Chemical Shift Constraints Obtained with High-Field 2-D and 3-D MAS NMR Dipolar Correlation Spectroscopy. *Biochemistry* **2001**, *40*, 1587−1595.
(64) Umetsu, M.; Hollander, J. G.; Matysik, J.; Wang, Z.-Y.; Adschiri, T.; Nozawa, T.; de Groot, H. J. M. Magic-Angle Spinning Nuclear Magnetic Resonance under Ultrahigh Field Reveals Two Forms of Intermolecular Interaction within CH2Cl2-Treated (31R)-Type Bacteriochlorophyll c Solid Aggregate. *J. Phys. Chem. B* **2004**, *108*, 2726−2734.
(65) Montaño, G. A.; Bowen, B. P.; LaBelle, J. T.; Woodbury, N. W.; Pizziconi, V. B.; Blankenship, R. E. Characterization of Chlorobium tepidum Chlorosomes: A Calculation of Bacteriochlorophyll c per Chlorosome and Oligomer Modeling. *Biophys. J.* **2003**, *85*, 2560−2565.
(66) Foidl, M.; Golecki, J. R.; Oelze, J. Bacteriochlorophyll c Formation and Chlorosome Development in Chloroflexus aurantiacus. *Photosynth. Res.* **1994**, *41*, 145−150.
(67) Arellano, J. B.; Psencik, J.; Borrego, C. M.; Ma, Y.-Z.; Guyoneaud, R.; Garcia-Gil, J.; Gillbro, T. Effect of Carotenoid Biosynthesis Inhibition on the Chlorosome Organization in Chlorobium phaeobacteroides Strain CL1401. *Photochem. Photobiol.* **2000**, *71*, 715−723.
(68) Shibata, Y.; Saga, Y.; Tamiaki, H.; Itoh, S. Polarized Fluorescence of Aggregated Bacteriochlorophyll *c* and Baseplate Bacteriochlorophyll *a* in Single Chlorosomes Isolated from Chloroflexus aurantiacus. *Biochemistry* **2007**, *46*, 7062−7068.
(69) Mimuro, M.; Nozawa, T.; Tamai, N.; Shimada, K.; Yamazaki, I.; Lin, S.; Knox, R. S.; Wittmershaus, B. P.; Brune, D. C.; Blankenship, R. E. Excitation Energy Flow in Chlorosome Antennas of Green Photosynthetic Bacteria. *J. Phys. Chem.* **1989**, *93*, 7503−7509.

(70) Miller, M.; Gillbro, T.; Olson, J. M. Aqueous Aggregates of Bacteriochlorophyll c as a Model for Pigment Organization in Chlorosomes. *Photochem. Photobiol.* **1993**, *57*, 98−102.
(71) Davydov, A. S. *Theory of Molecular Excitons*; Plenum Press: New York, London, 1971.
(72) Shipman, L. L.; Katz, J. J. Calculation of the Electronic Spectra of Chlorophyll a- and Bacteriochlorophyll a-Water Adducts. *J. Phys. Chem.* **1977**, *81*, 577−581.
(73) Agranovich, V. M.; Galanin, M. D. *Electronic Excitation Energy Transfer in Condensed Matter*; North-Holland Publishing Company: Amsterdam, The Netherlands, 1982.
(74) Zazubovich, V.; Tibe, I.; Small, G. J. Bacteriochlorophyll *a* Franck-Condon Factors for the S0 → S1(Q*y*) Transition. *J. Phys. Chem. B* **2001**, *105*, 12410−12417.
(75) Martiskainen, J.; Kananavicius, R.; Linnanto, J.; Lehtivuori, H.; Keränen, M.; Aumanen, V.; Tkachenko, N.; Korppi-Tommola, J. Excitation Energy Transfer in the LHC-II Trimer: From Carotenoids to Chlorophylls in Space and Time. *Photosynth. Res.* **2011**, *107*, 195−207.
(76) Knox, R. S.; Spring, B. Q. Dipole Strengths in the Chlorophylls. *Photochem. Photobiol.* **2003**, *77*, 497−501.
(77) Pearlstein, R. M. In *Chlorophylls*; Scheer, H., Ed.; CRC Press: Boca Raton, FL, 1991; p 1047.
(78) Mauring, K.; Novoderezhkin, V.; Taisova, A.; Fetisova, Z. Exciton Levels Structure of Antenna Bacteriochlorophyll c Aggregates in the Green Bacterium Chloro£exus aurantiacus as Probed by 1.8-293 K Fuorescence Spectroscopy. *FEBS Lett.* **1999**, *456*, 239−242.
(79) Korppi-Tommola, J. E. I.; Linnanto, J. M. An Exciton Model to Calculate Spectra, Intra- and Intercomplex Energy Transfer Rates of Photosynthetic Light Harvesting Antenna. *PS2001 Proceedings 12th International Congress on Photosynthesis*, CSIRO Publishing (ISBN: 0643067116), 2002.
(80) Ihalainen, J. A.; Linnanto, J.; Myllyperkiö, P.; van Stokkum, I. H. M.; Ücker, B.; Scheer, H.; Korppi-Tommola, J. E. I. Energy Transfer in LH2 of Rhodospirillum molischianum, Studied by Subpicosecond Spectroscopy and Configuration Interaction Exciton Calculations. *J. Phys. Chem. B* **2001**, *105*, 9849−9856.
(81) Förster, Th. In *Modern Quantum Chemistry Istanbul Lectures, Part III: Action of Light and Organic Crystals*; Sinanoğlu, O., Ed.; Academic Press: New York, 1965; p 93.
(82) Fetisova, Z. G.; Mauring, K. Experimental Evidence of Oligomeric Organization of Antenna Bacteriochlorophyll c in Green Bacterium Chloroflexus aurantiacus by Spectral Hole Burning. *FEBS Lett.* **1993**, *323*, 159−162.
(83) Fetisova, Z.G.; Mauring, K.; Taisova, A.S. Strongly Exciton-Coupled BChl e Chromophore System in the Chlorosomal Antenna of Intact Cells of the Green Bacterium Chlorobium phaeovibrioides: A Spectral Hole Burning Study. *Photosynth. Res.* **1994**, *41*, 205−210.
(84) Caffarri, S.; Kouril, R.; Kereiche, S.; Boekema, E. J.; Croce, R. Functional Architecture of Higher Plant Photosystem II Supercomplexes. *EMBO J.* **2009**, *28*, 3052−3063.
(85) Ma, Y.-Z.; Cogdell, R. J.; Gillbro, T. Energy Transfer and Exciton Annihilation in the B800-850 Antenna Complex of the Photosynthetic Purple Bacterium *Rhodopseudomonas acidophila* (Strain 10050). A Femtosecond Transient Absorption Study. *J. Phys. Chem. B* **1997**, *101*, 1087−1095.
(86) Strümpfer, J.; Schulten, K. Light Harvesting Complex II B850 Excitation Dynamics. *J. Chem. Phys.* **2009**, *131*, 225101-1−225101-9.
(87) Linnanto, J. M.; Korppi-Tommola, J. E. I. Modelling Excitonic Energy Transfer in the Photosynthetic Unit of Purple Bacteria. *Chem. Phys.* **2009**, *357*, 171−180.